ORIGINAL RESEARCH PAPER

Implications of the 2011 M9.0 Tohoku Japan earthquake for the treatment of site effects in large earthquakes

Hadi Ghofrani · Gail M. Atkinson · Katsuichiro Goda

Abstract   Site response in Japan is characterized using thousands of surface and borehole recordings from events of moment magnitude (M) > 5.5 collected by the KiK-net network, including the 2011 M9.0 Tohoku earthquake. Site amplification is defined by the ratio of motions at the surface to those at depth (within the borehole), corrected for the depth effect due to destructive interference using a technique based on cross-spectral ratios between surface and down-hole motions. Site effects were particularly strong at high frequencies, despite the expectation that high-frequency response may be damped by nonlinear effects. In part, the large amplitudes at high frequencies are due to the prevalence of shallow soil conditions in Japan. We searched for typical symptoms for soil nonlinearity, such as a decrease in the predominant frequency and/or amplification, using spectral ratios of weak to strong ground motions. Localized nonlinearity occurred at some recording sites, but was not pervasive. We developed a general empirical model to express site amplification for the KiK-net sites as a function of common site variables, such as the average shear-wave velocity in the uppermost 30 m (V_{S30}) and the horizontal-to-vertical (H/V) spectral ratio. We use the model to estimate site-corrected ground-motions for the Tohoku mainshock for a reference site condition; these motions are in reasonable agreement with the predictions of some of the published ground motion prediction equations for subduction zones.

Keywords   Site effects, Soil nonlinearity · Surface-to-borehole cross-spectral ratio · Horizontal-to-vertical spectral ratio · Ground-motion prediction equation

H. Ghofrani (✉)· G. M. Atkinson
Department of Earth Sciences, Western University, London, ON N6A 5B7, Canada
e-mail: ghofrani_hadi@yahoo.com

G. M. Atkinson
e-mail: Gmatkinson@aol.com

K. Goda
Department of Civil Engineering, University of Bristol, Bristol, UK

1 Introduction

Site amplification, or the increase in amplitudes of seismic waves as they traverse soft soil layers near the Earth's surface, is a major factor influencing the extent of earthquake damage to structures (Borcherdt 1970; Nakamura 1989; Lermo and Chávez-García 1994; Field and Jacob 1995). Thus understanding of site-specific amplification effects and their role in determining ground motions is important for the design of engineered structures. The methods utilized for site effect analysis from recorded motions can be divided into three general approaches. A standard spectral ratio (SSR) approach has been applied to determine the ratio of the motions recorded on a soil site to those recorded on a nearby reference rock site (Borcherdt 1970; Hartzell 1992; Field and Jacob 1995; Kato et al. 1995; Field 1996; Hartzell et al. 1996; Su et al. 1996; Bonilla et al. 1997). In this method, it is assumed that the reference rock site does not amplify ground motion. However, it is difficult to find a true reference site due to the prevalence of a weathered layer near the surface everywhere (Steidl et al. 1996); the reference rock site may also have significant amplification due to impedance effects associated with its shear-wave velocity gradient. Moreover, if the reference rock site is not very close to the target soil site, then the incident wave field may not have the same characteristics. Other variants of the spectral ratio approach include the use of cross-spectral ratios (Safak 1991; Steidl 1993), response spectral ratios (Kitagawa et al. 1992), ratios of peak RMS (root-mean-square) or effective accelerations (Borcherdt and Wentworth 1995), and blind deconvolution techniques (Zerva et al. 1995).

The second method uses generalized inversion techniques to characterize site amplification. In this method, the source, path, and site characteristics are identified simultaneously (Andrews 1986; Boatwright et al. 1991; Hartzell 1992); reviews of this method can be found in Bard (1994) and Field and Jacob (1995). The advantage of this method is in providing the absolute amplification/de-amplification of body waves (S-wave) at a site. However, like the SSR technique, the generalized inversion method also suffers from the need to define a reference site.

The third common method of quantifying the site effects is known as the single-station method (Langston 1979; Nakamura 1989). This technique is based on the horizontal-to-vertical spectral ratio of the motions at a site, which is convenient in cases where no reference site is available. Reviews of this method can be found in Lachet and Bard (1994), Field and Jacob (1995), and Atakan (1995).

In this study, we use a technique based on cross-spectral ratios, a more direct variant of the SSR approach, in which the reference site is at the bottom of a borehole, directly below the soil site. Borehole data are useful in measuring site effects. For example, borehole measurements have provided direct in situ evidence of nonlinearity (Seed and Idriss 1970; Wen et al. 1994; Zeghal and Elgamal 1994; Iai et al. 1995; Sato et al. 1996; Aguirre and Irikura 1997; Satoh et al. 2001a); for surface-rock recordings they can be used as input motion to soil columns (Satoh et al. 1995; Steidl et al. 1996; Boore and Joyner 1997); and they have provided information about scaling of earthquakes of different magnitudes (Kinoshita 1992; Abercrombie 1997). The problems associated with using borehole data as the input to a site transfer function were discussed by Cadet et al. (2012). The most significant effect is the interference between the incident wave and the reflection from the surface and any other velocity contrasts (discontinuities) in the soil column. The destructive interference of the incident wave field and the down-going waves may produce holes in the ground-motion spectral ratio (Steidl et al. 1996). Consequently, a direct spectral ratio between the surface and the total motion at depth generally produces pseudo-resonances where these holes are present. These phenomena are referred to as the depth effect (Cadet et al. 2012).
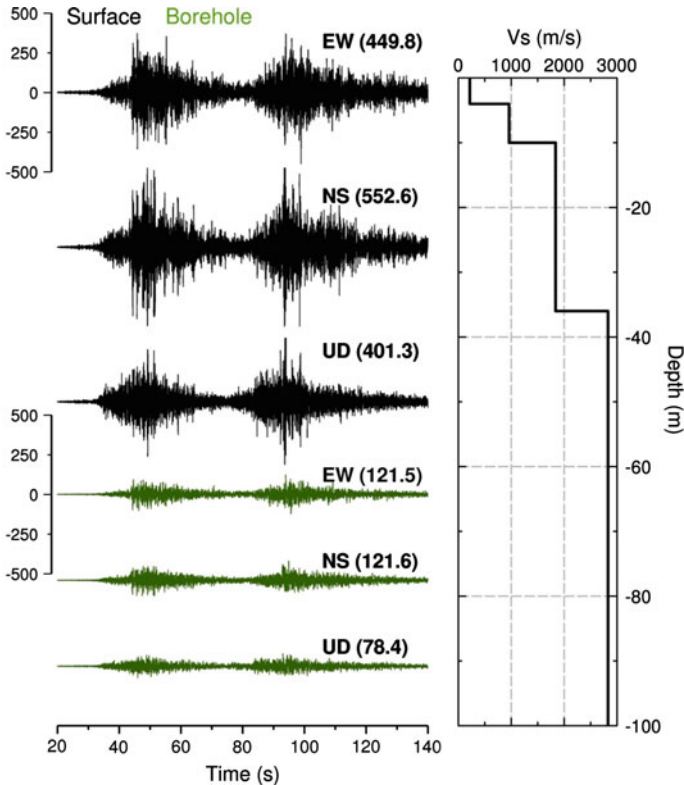
Fig. 1 Comparison of observed surface and borehole ground motions for MYGH04 station of the KiK-net. The values at the end of each trace list the peak ground acceleration in cm/s^2 for East-West (EW), North–South (NS), and Vertical (UD) components, respectively. All the records are plotted on the same scale. Time series in black are recorded on the surface, and those in green are recorded in the borehole. The plot on the right is the shear-wave velocity profile of the corresponding site. The site is at $\sim$ 91 km from the fault plane and categorized as the NEHRP site class C (very dense soil and soft rock), with $V_{S30} = 850$ m/s. Seismometer is installed at depth of 100 m at this station

These effects should be taken into account when using surface-to-borehole spectral ratios (S/B) for computing the transfer function of a site, though the best means of doing so is a controversial issue.

Site amplification effects were profound for the 2011 **M**9.0 Tohoku event. As an illustration, Fig. 1 compares surface and borehole ground motions at station MYGH04; the location of this station relative to the fault plane is indicated by a black square in Fig. 2. Amplitudes of ground motions at the borehole level (PGA[borehole] $\approx$ 100 cm/s^2) are amplified by a factor of 5 at the surface (PGA[surface]); this large amplification is due to the presence of a shallow low-velocity soil layer, about 4 m thick, that overlies stiff bedrock.

In this study, we perform a thorough analysis of site amplification during the Tohoku event (as well as other Japanese events of **M** $>$ 5.5). We take advantage of the vertical array of the KiK-net (KIBAN kyoshin network: http://www.kik.bosai.go.jp/) including the enriched database of the NIED (National Research Institute for Earth Science and Disaster Prevention: http://www.bosai.go.jp/e/) to estimate the site transfer functions for all sites,
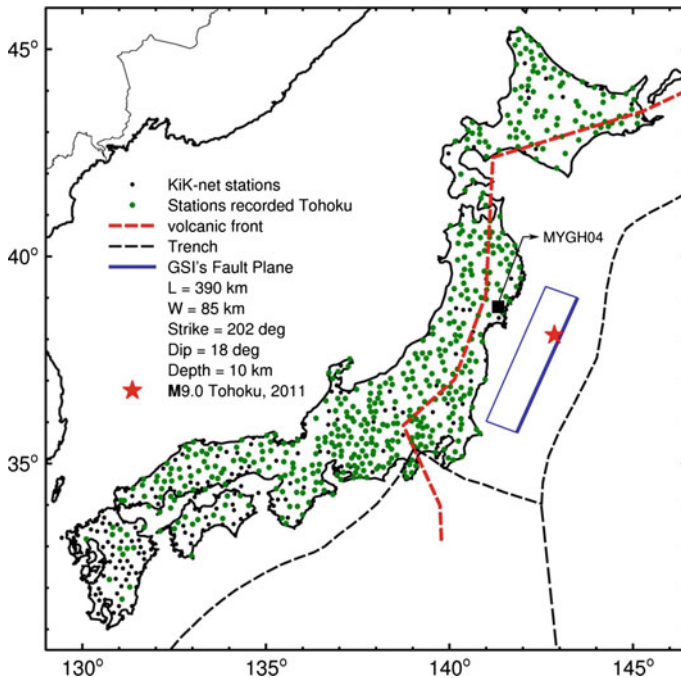
Fig. 2 The spatial distribution of all KiK-net stations (*black dots*) and those stations recorded the Tohoku event (*green dots*). The *star* is the epicenter. The major tectonic boundaries—the trench and the volcanic front—are represented by *dashed black* and *red lines*, respectively. A *blue rectangle* shows the fault plane obtained from the GPS Earth Observation Network System (GEONET) data analysis (http://www.gsi.go.jp/)

considering both linear and nonlinear site effects. The applicability of the H/V spectral ratio technique as an alternative tool to estimate site response is evaluated by modeling the relationship between H/V ratios and S/B ratios, as a function of physical site properties. We examine several approaches for site amplification estimation, as a means of checking the robustness of the functions we determined based on S/B ratios. We develop a suite of simple, useful, and reliable models for prediction of site amplification effects based on readily-obtainable site parameters. Finally, we develop an empirical model of ground motions for the Tohoku earthquake (including site effects) and compare it to the predictions of several existing ground motion prediction equations (GMPEs) commonly used in seismic hazard analysis applications.

## 2 Strong ground motion data and record processing

The strong-motion data used in this study were collected from the KiK-net of the NIED of Japan. The KiK-net consists of 687 strong-motion observation stations installed both on the ground surface and at the bottom of boreholes (directly below the surface site). Figure 2 shows the distribution of the KiK-net stations triggered by the Tohoku event. Detailed descriptions of the other strong motion networks that recorded ground-motions of the 2011 Tohoku earthquake can be found in Aoi et al. (2011) and Midorikawa et al. (2012).

To enable a statistically-robust and meaningful analysis of site effects, we supplement the Tohoku-event data by adding other events of $M \geq 5.5$ that were recorded on all KiK-net stations from 1998 to 2009. For the 687 KiK-net stations, we have processed and analyzed 30,453 records from 258 earthquakes in total. The number of events for each station varies from 4 to 150. The processing procedure for all records includes windowing, correction for baseline trend, and band-pass filtering. We have applied non-causal, band-pass Butterworth filters with an order of 4. The selected frequency range of analysis is 0.1–15 Hz. The lower frequency limit was selected by inspecting many records, and concluding that this value is appropriate to produce well-shaped displacement time series, with a flat portion of the displacement spectrum at low frequencies. The upper limit is chosen by considering the cut-off frequency of the seismograph response spectrum (15 Hz). For each record, we compute the instrument-corrected Fourier amplitude spectrum (FAS) of accelerograms.

3 Calculation of site response using surface-to-borehole spectral ratio (S/B)

Surface-to-borehole spectral ratios (S/B) are used to provide a direct measure of site response. However, destructive interference between the up-going incident wave field and down-going reflected waves from the surface at specific frequencies can produce a notch in the FAS of the borehole recording (Shearer and Orcutt 1987; Steidl et al. 1996). For an undamped single layer over an elastic half space, this notch can be interpreted as the infinite value of the transfer function (Zhao 1996) between the total displacement at the surface soil site and the total displacement at the bottom of the soil layer (borehole record) (J. Zhao, personal communication, 2012). The existence of this hole in the borehole spectrum could produce peaks in the spectral ratios that might be misinterpreted as site-response peaks. Figure 3 schematically illustrates the problem. In this figure, the amplitude spectrum of incident waves is denoted "A", while that of the reflections is denoted "B". It is assumed that the soil profile consists of n layers overlying bedrock. As the incident and reflected waves always constructively interfere at the surface, the total amplitude for the outcrop rock would be $2A_n$, while for the station over the soil column it would be $2A_1$. The ratio of motions recorded at the surface on soil to those on bedrock can be defined as:

$$\frac{S}{B} = \frac{2A_1}{(A_n + B_n)} \tag{1}$$
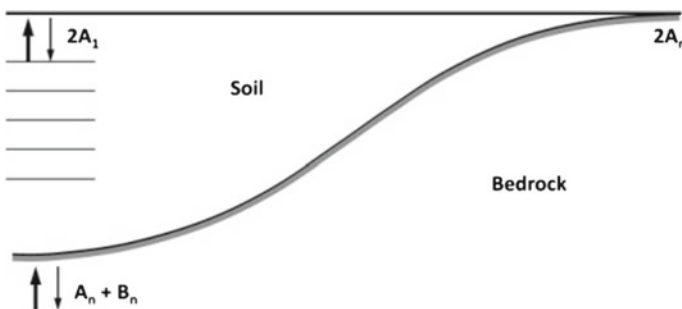
Fig. 3 Schematic representation of site amplification. Soil profile consists of n layers where incident and reflected waves for each layer are denoted as A_i and B_i (i = 1 to n), respectively. Amplification can be defined as the surface-to-borehole (S/B) spectral ratio [Eq. (1)] or surface-to-outcrop (standard) spectral ratio (SSR: $2A_1/2A_n$)

The factor of two in the numerator represents the free-surface amplification. At the borehole level, the down-going reflected waves are interfering destructively and will reduce the apparent amplitude of the incident waves, thus obscuring the actual site response.

A possible solution to the destructive interference problem involves the use of cross-spectrum techniques (Safak 1991; Field et al. 1992; Steidl 1993; Bendat and Piersol 2006), which consider the coherency of the waveforms at the surface and down-hole. Taking into account the effect of the reflected wave-field, S/B ratios are multiplied by the coherence (C^2) between surface and borehole recordings (Steidl et al. 1996). The coherence is defined as:

$$C^2 = \frac{|S_{12}(f)|^2}{S_{11}(f)\, S_{22}(f)'} \tag{2}$$

and thus the depth-corrected cross spectral ratios are given by:

$$S/B' = C^2 (S/B), \tag{3}$$

where $S_{11}(f)$ and $S_{22}(f)$ are the power spectral densities of the seismograms recorded at the surface and down-hole, respectively, $S_{12}(f)$ is the cross-power-spectral density function (Steidl et al. 1996), and S/B′ is the S/B ratio corrected for the depth effect. It should be mentioned that a loss in coherence could be due to the site response itself, and not just to the destructive interference effect.

Another possible way to correct the S/B ratio for the depth effect is to use empirical correction factors as proposed by Cadet et al. (2012). The correction function in their paper is an empirical version of an analytical solution provided by Zhao (1996; 1997) for a multiple-layer 1-D model. The key parameter in the correction factors is the fundamental resonance frequency (f_0) of a site. In their paper, the fundamental resonance frequency was defined as the frequency corresponding to the first (i.e., lowest frequency) peak of the S/B ratio. A "peak" is defined as a specific local maximum with amplitude larger than 2 in a statistical sense (Cadet et al. 2012). Knowing the average shear-wave velocity (V_S) over the depth of the borehole (D_b), the so-called first destructive interference frequency (f_{d1}) of the soil column can also be estimated using $f_{d1} = V_S/4D_b$.

To illustrate the issues, Fig. 4 shows recorded FAS and S/B ratios for two representative sites (ABSH10 and AICH12). Based on the definition of f_0 given by Cadet et al. (2012) (i.e. the lowest frequency peak with amplitude > 2), we might choose $f_0 \sim 2.0\,$Hz for both stations. Referring to Fig. 4, we can see that the increase in the amplitude of S/B for ABSH10 near 2.0 Hz is due to a corresponding drop of FAS at the borehole level because of downward reflections. However, the significant amplification at the surface in AICH12 near 2.0 Hz is clearly due to actual site amplification; it is not due to interference of incident and reflected waves at the borehole, and should therefore not be reduced using correction factors. We found that, in general, empirical correction factors and cross-spectral ratio techniques produced similar results in terms of eliminating the depth effect. However, we adopt the cross-spectral ratio techniques to calculate S/B′ (as defined by Eq. (3)) as it is easier to apply and less subject to misinterpretations (Fig. 4). We acknowledge that there is some controversy in the best approach to correct S/B ratios for the depth effect, and even in the meaning of the spectral holes that can be seen in S/B ratios (J. Zhao, personal communication, 2012). Therefore, we have used several lines of reasoning to investigate the robustness of our S/B′ ratios as a measure of the site transfer function.

One check on the amplifications derived using S/B′ ratios is to compare them to those computed theoretically based on the site soil profile. In order to estimate the theoretical site response we used the program Nrattle (written by C. Mueller with modification by R. Herrmann), which calculates the 1-D transfer function of a layered, damped soil over
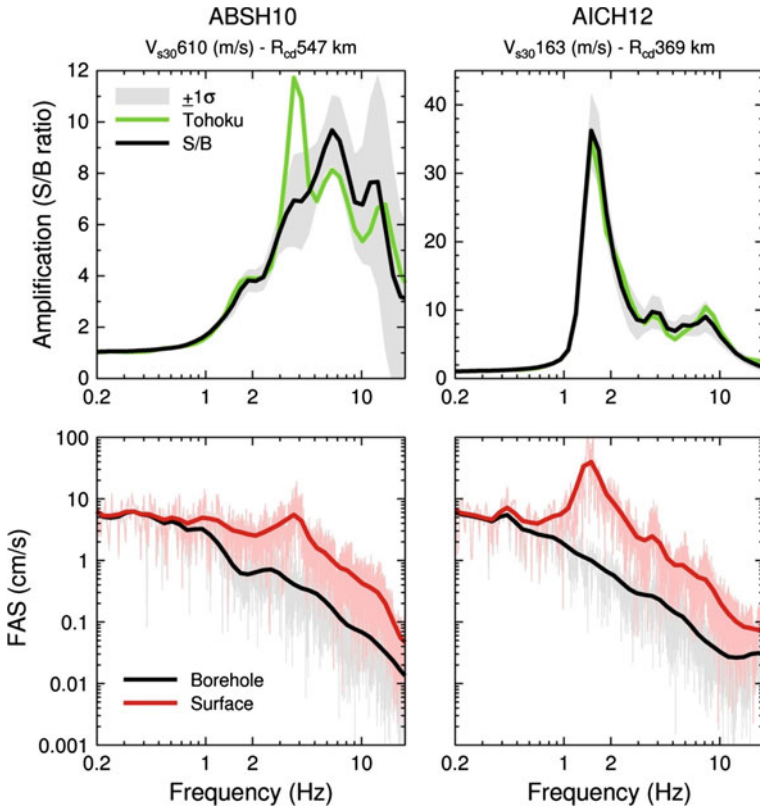
Fig. 4 Comparing the amplification functions at two different stations. The *top row* is showing S/B ratio (*horizontal component*) for the Tohoku event data (*green line*) along with the corresponding average for all KiK-net data (*solid black line*), and its ± 1σ bounds (*shaded gray*). The *bottom row plots* the FAS of *horizontal components* (geomean) for Tohoku, for both surface and borehole ground motions. The *solid lines* are the smoothed spectra

an elastic bedrock, for a vertically propagating shear-wave (SH), using a Thomson–Haskell approach (Thomson 1950; Haskell 1960). The Nrattle solution was found to be exactly equivalent to the solution computed by the equivalent-linear site response program SHAKE (Schnabel et al. 1972) for linear modulus reduction and damping curves (Thompson et al. 2009). The input data for Nrattle are the layered velocity model, specifying the thickness, density, shear-wave velocity, and Quality factor for each layer. For the density and Quality factor, we used values reported by Cadet et al. (2012). The other input parameters are the velocity and density of the half-space, incident angle, and the depth with respect to which the transfer function is calculated. This reference depth is the depth of installation for borehole sensors. We compared the fundamental frequencies and amplitude of amplification as obtained from the theoretical transfer function with the corresponding values as deduced from the S/B′ ratios (after correction for the depth effect), for 167 sites where there is a clear, statistically-significant single peak in the H/V ratios. We found close correlation between the theoretical transfer functions and observations, in agreement with similar results from other studies (Steidl et al. 1996; Cadet et al. 2012). Observed and predicted fundamental frequencies are strongly correlated (correlation coefficient of 0.95), with standard deviation

of residuals (empirical S/B′—theoretical S/B′) of $\sigma_{residual} = 0.08$ (log base 10). The agreement between S/B′ and theoretical amplification amplitude is not as close as that for the fundamental frequencies, with a mean residual of almost zero and $\sigma_{residual} = 0.23$. The greater scatter between observed and theoretical site response amplitudes could be the result of errors in the parameters specifying the velocity profiles, densities, and Quality factors used for computing the transfer functions.

Good agreement with the results obtained by the cross-spectral ratios (S/B′) from this study and the empirical correction factors using the techniques of Cadet et al. (2012) further indicates the robustness of our calculated site response functions; correlation coefficients at almost all frequencies are greater than 0.8 (for frequencies > 0.4 Hz, correlation coefficients are greater than 0.9). It should be mentioned that S/B′ ratios may not represent the desired transfer function for sites with significant feedback at the borehole sensor (Safak 1991, 1997). Nonetheless, this is not the case for many sites as shown in Fig. 4. On the other hand, Safak (1997) illustrated that S/B′ ratios provide probabilistically more accurate estimates than the traditional SSR ratios by proving that they represent the least-squares estimate of site amplification if noise signals are assumed to be Gaussian random processes (Assimaki et al. 2008).

Finally, we checked key aspects of the transfer function using empirical regression (as in a traditional GMPE) to determine the amplification term for V_{S30} (relative to a reference of 760 m/s). This confirmed that the amplifications via S/B′, which applies to stations with shear-wave velocity at the bottom of the borehole ($V_S[depth]) \geq 760$ m/s), and via regression for the same condition give similar peak and frequency.

4 Relationship between amplification and site parameters

4.1 Linear site amplification

In this section, we examine the relationship between site amplification (as given by S/B′ ratios) and site variables describing the depth and stiffness of the deposit. As a commonly-used index parameter for the shear-wave velocity profile, we use the average shear-wave velocity in the uppermost 30 m (Borcherdt 1992, 1994):

$$V_{S30} = 30 \left/ \sum_{i=1}^{N} \left(\frac{d_i}{v_i} \right) \right. , \tag{4}$$

where d_i and v_i denote the thickness (in meters) and shear-wave velocity of the ith layer respectively, and N is the total number of layers. To calculate V_{S30} for each site, we use the site velocity profile of the KiK-net stations, extended to the depth of 100–200 m as recommended by Boore et al. (2011).

Figure 5 explores the relationship between site amplification and V_{S30}, considering all KiK-net data. In this figure, $V_S[depth]$ is the value at the depth of installation; we assume that, for holes that extend to hard-rock conditions ($V_S > 1,500$ m/s), the vertical component at that depth is essentially unamplified, and the horizontal component has only a small potential amplification (as represented by the H/V ratios at the bottom). As seen in Fig. 5, the average S/B′ ratio increases with frequency, as does the scatter among data points. We see some evidence for greater amplification, for the same V_{S30}, if $V_S[depth] \geq 760$ m/s, due to impedance effects. Furthermore, the amplification for the data in the range 760–1,500 m/s appears to be similar to that for $V_S[depth] > 1,500$ m/s. We therefore conclude that for
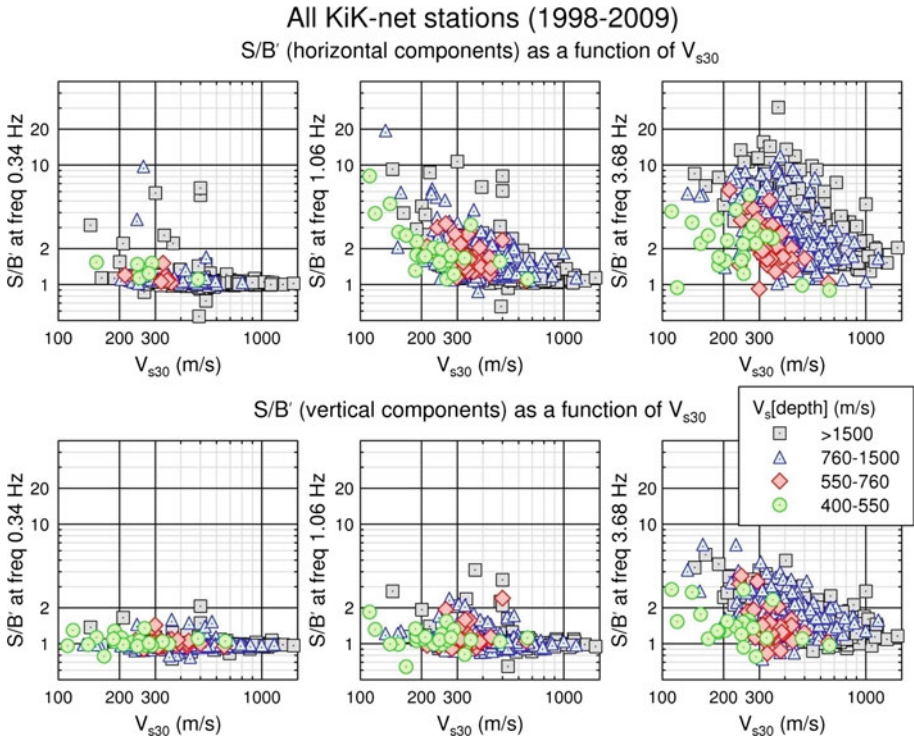
Fig. 5 Amplification S/B′ (*horizontal components*) for the KiK-net stations relative to V_{S30}, using all events from 1998 to 2009. Sites are categorized into four groups based on their V_S[depth] which is shear-wave velocity at the depth of installation. The amplification of the *vertical component* S/B′(vert) is also plotted versus V_{S30}

characterizing the overall site amplification, we should use the S/B′ ratio data for V_S[depth] ≥ 760 m/s. We perform a simple least-squares regression to determine the amplification for each frequency as a function of V_{S30}:

$$\log_{10}\left(S/B'\right) = m.\log_{10}\left(V_{S30}/V_{ref}\right) + b, \tag{5}$$

where $V_{ref} = 760$ m/s. This regression will give us an estimate of the site term to remove from the data, if we wish to correct them to equivalent values for bedrock, $V_{S30} = 760$ m/s (B/C boundary site conditions according to the National Earthquake Hazard Reduction Program, NEHRP, provisions) in a generic way. The regression coefficients (amplification factors) are tabulated in Table 1 for the frequency range of 0.1–15 Hz. Table 1 contains site amplification coefficients using just the Tohoku event and those obtained using all KiK-net data ($\mathbf{M} \geq 5.5$; 1998–2009).

Another important site parameter, in addition to site stiffness, is the fundamental resonance frequency. The fundamental frequency depends on both layer depth and its stiffness. The mapping of predominant frequency of amplification facilitates the micro-zonation (Lachet and Bard 1994). Furthermore, the fundamental frequency may carry information on deeper part of the soil column, in comparison to V_{S30} which considers only the top 30 m. The fundamental frequency is obtained for the KiK-net data using the peak of the H/V spectral ratios of the recorded strong motions at the sites (Lermo and Chávez-García 1993;

**Table 1** Coefficients for site correction factors, horizontal component

Frequency (Hz)	Period (s)	Tohoku		All KiK-net	
		m	b	m	b
0.11	9.09	−0.0313	0.0086	−0.0526	−0.0372
0.14	7.14	−0.0450	0.0086	−0.0491	−0.0184
0.17	5.88	−0.0610	0.0099	−0.0577	−0.0087
0.22	4.55	−0.1091	0.0085	−0.0904	−0.0020
0.27	3.70	−0.1378	0.0099	−0.1165	0.0031
0.33	3.03	−0.1509	0.0157	−0.1284	0.0096
0.41	2.44	−0.1791	0.0203	−0.1516	0.0160
0.52	1.92	−0.2475	0.0270	−0.2113	0.0233
0.64	1.56	−0.3296	0.0346	−0.2862	0.0307
0.80	1.25	−0.4211	0.0458	−0.3745	0.0421
0.99	1.01	−0.5182	0.0629	−0.4908	0.0547
1.23	0.81	−0.6125	0.0851	−0.6064	0.0754
1.53	0.65	−0.6814	0.1189	−0.6813	0.1087
1.90	0.53	−0.7476	0.1571	−0.7681	0.1478
2.37	0.42	−0.8310	0.1954	−0.8778	0.1867
2.94	0.34	−0.8337	0.2374	−0.9109	0.2326
3.66	0.27	−0.6868	0.3004	−0.8270	0.2983
4.55	0.22	−0.6220	0.3378	−0.7239	0.3573
5.66	0.18	−0.4979	0.3836	−0.5965	0.4108
7.04	0.14	−0.2755	0.4292	−0.4059	0.4623
8.75	0.11	−0.0759	0.4467	−0.2051	0.4945
10.88	0.09	0.0566	0.4381	−0.0138	0.4900
13.53	0.07	0.1957	0.3745	0.2258	0.4541

m and b are the regression coefficients using data for V_S[depth] $\geq$ 760 m/s

Theodulidis and Bard 1995; Zhao et al. 2006a; Fukushima et al. 2007), considering all events of **M** $\geq$ 5.5 recorded at each station from 1998 to 2009. Only those stations that recorded at least three events are considered. The peak of the H/V ratios may be ambiguous as an indicator of fundamental frequency in the case of close proximity to sources or in the absence of a marked impedance contrast at some depth. However, when averaged over multiple events, the peak H/V ratio provides a stable estimate of fundamental frequency that is well-correlated with that obtained from the peak of the S/B′ ratio.

Considering all events recorded at each station, we have calculated the mean value of horizontal-to-vertical spectral ratios at both surface H/V[surface] and at the bottom of the borehole H/V[depth]. The latter is helpful in detecting the possible presence of a large impedance contrast at deeper sections of the borehole. To determine the H/V ratios, the following procedure was applied:

1) Apply a 5% cosine taper function to the signal window;
2) Calculate FAS of the three components (NS, EW, UD), for both surface and borehole ground-motions;
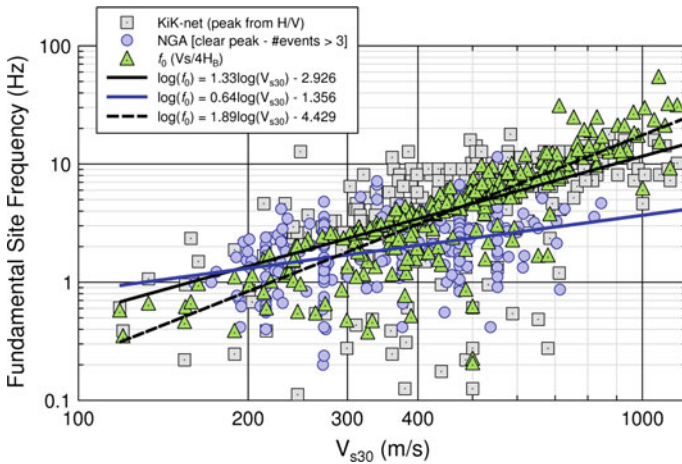
Fig. 6 Fundamental site frequency as a function of V_{S30}. *Gray squares* are observations for which a clear peak frequency is indicated by the H/V ratio. The *green triangles* are fundamental site frequencies calculated using the equation $f_0 = V_S/4H_B$, where H_B is the known depth-to-bedrock. The blue circles are observed fundamental frequencies of NGA data. *Lines* are the best linear fit to f_0 as a function of V_{S30} for each dataset

3) Smooth the FAS using a Konno-Ohmachi window with a bandwidth parameter, b, of 20 (Konno and Ohmachi 1998);
4) Obtain the geometric mean of the two horizontal components $((FAS_{EW} \times FAS_{NS})^{0.5})$;
5) Calculate the ratio of FAS(H) to FAS(V) at the surface and the borehole (H/V[surface] and H/V[depth]).

Despite varying amplitudes and predominant frequencies, the H/V[surface] ratios can be grouped based on their overall shape. About 60 % of the stations show a single clear H/V "peak" which is associated with the fundamental frequency of the site; a peak is defined as a local maximum where the amplitude is greater than twice the mean level of H/V[surface]. The rest of the spectral ratios can be divided into groups having two peaks (20 %), more than two peaks (jagged shape), or no significant peak.

At the bottom of the borehole, we would expect H/V[depth] to be unity, if this is at bedrock level (Nakamura 1989; Theodulidis et al. 1996). However, for the KiK-net stations the borehole sensor is not always placed at bedrock. By inspection of H/V[depth] compared to H/V[surface], there are often peaks at very low-frequencies, which could be due to significant velocity contrast beneath the down-hole sensor (Cadet et al. 2012).

We would expect the fundamental frequency to be related to the depth-to-bedrock (i.e. $f_0 = V_S/4H_B$; Dobry et al. 2000). The depth-to-bedrock, defined by the depth of a layer with $V_{S\geq}760$ m/s, or to a significant impedance contrast between surface soil deposits and material with $V_S \cong 760$ m/s, is obtained for each site from the velocity profile. Figure 6 plots the fundamental site frequency as a function of V_{S30}. As V_{S30} is a common site parameter in engineering seismology, its relationship with other site parameters is important and useful. It is interesting that V_{S30} appears to be a good proxy to estimate the natural frequency of a site. Furthermore, the fundamental frequency inferred from the H/V ratios matches well with that derived from the theoretical relation ($f_0 = V_S/4H_B$). Strictly speaking, this expectation is only true for a soil layer with a constant V_S profile over a thickness of H_B. The frequency $f_0 = V_S/4H_B$ is also close to the first modal frequency for a layered 1-D site. It is worth pointing out that the correlation between V_{S30} and f_0 is not applicable for deep low-frequency
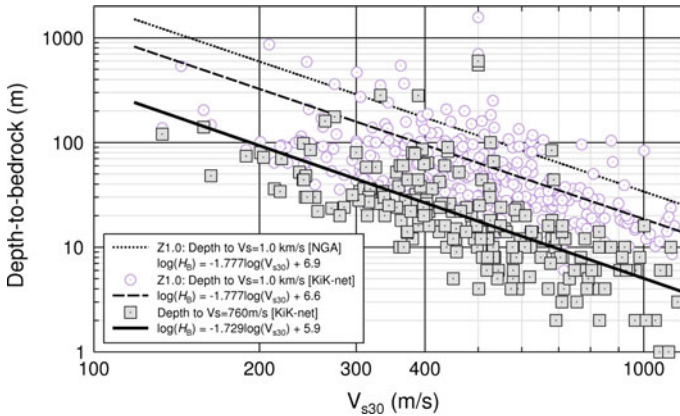
Fig. 7 Depth-to-bedrock as a function of V_{S30}. *Gray squares* are the depth to $V_S = 760$ m/s and *purple circles* are Z1.0 (depth to $V_S = 1,000$ m/s) from velocity profiles of the KiK-net stations. The *dotted line* is the best fit to the Z1.0 values from the PEER-NGA database. The *dashed line* is the estimated model for predicting Z1.0 in Japan. Note deeper bedrock for the PEER-NGA database

sites (Zhao and Xu 2012b). In Fig. 6, the upper limit on site frequency at 10 Hz may be artificial due to the limitations of the instruments and filtering - we would not be able to see peaks at shorter periods clearly.

To check if the V_{S30}-f_0 correlation is region-specific, or the observed relation may be valid in other tectonic regions, we use the 2005 Pacific Earthquake Engineering Research Center (PEER) ground motion database which was developed for the 2008 NGA-West project (http://peer.berkeley.edu/smcat/). The PEER-NGA database is the most complete source of high-quality ground-motion data compiled from active tectonic regions. The database consists of 3,551 multi-component records from 173 shallow crustal earthquakes (**M**4.2–7.9). We calculate the H/V ratios for all sites in the database and pick the fundamental frequencies, considering just those stations that show a clear single peak and that recorded at least 3 events. As there are relatively few NGA stations having multiple recordings, the slope of the V_{S30}-f_0 relation is less significant (0.64 ± 0.10) than that for Japan (1.33 ± 0.12). The systematically-lower values of f_0 for the NGA data, in comparison to the Japanese data, can be attributed to deeper bedrock (for the same V_{S30}) for most regions that comprise the NGA database; about 75 % of the NGA data we used in this study are from the 1999 Chi–Chi, Taiwan earthquake. It should be noted that the KiK-net stations are intentionally sited on harder sites, not deeper soil sites.

Figure 7 plots the fundamental site frequency as a function of depth-to-bedrock, which is interrelated to V_{S30}. We also show in Fig. 7 the corresponding relationship for the PEER-NGA strong motion dataset; for the PEER-NGA data, the "depth to bedrock" is assumed to be the depth to $V_S = 1.0$ km/s (Z1.0), as it is the closest proxy to our selected $V_S = 760$ m/s. The Japanese and PEER-NGA data show similar trends, but there is a greater intercept for the PEER-NGA data, probably because they are referenced to stiffer, deeper bedrock. We also show the estimated Z1.0 from the velocity profiles of the KiK-net stations in Fig. 7. We find that with an approximate adjustment, one can estimate Z1.0 in Japan and California by using the V_{S30} and depth-to-bedrock relation for Japan. The correlations for fundamental site frequency and depth-to-bedrock (H_B) with V_{S30} can be described for Japan by the following linear regressions:
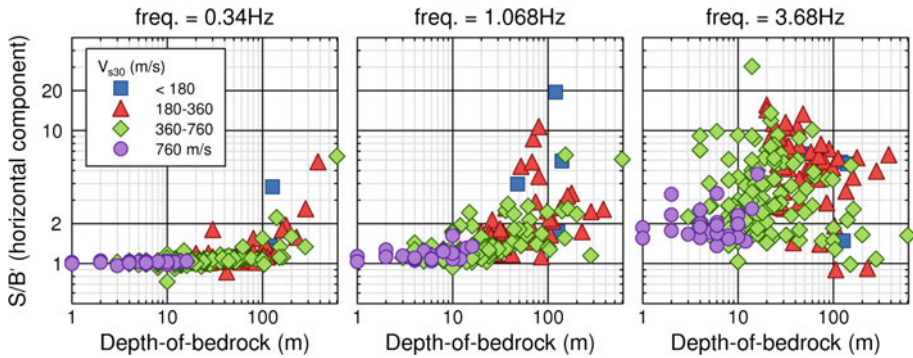
Fig. 8 Corrected site amplifications (*horizontal components*) versus depth-to-bedrock, at frequency = 0.34, 1.1, and 3.7 Hz. The symbols are binned into different groups based on V_{S30}

$$\log_{10}(f_0) = 1.331 \log_{10}\left(\frac{V_{S30}}{V_{ref}}\right) + 0.9066, \tag{6}$$

$$\log_{10}(H_B) = -1.729 \log_{10}\left(\frac{V_{S30}}{V_{ref}}\right) + 0.9136 \tag{7}$$

In Fig. 8, we examine the factors influencing site amplification, specifically depth-to-bedrock, and V_{S30}. At low frequencies, as we would expect, the large wavelengths see (sample) only deep deposits. At higher frequencies, we are sampling more of the near-surface materials. Note that shallow sites are relatively stiff in terms of V_{S30}, and generally show less amplification (except for shallow soil sites at high frequency). We developed empirical relationships between site amplification (S/B′), depth-to-bedrock and fundamental site frequency, of the following form:

$$\log_{10}\left(S/B'\right) = a.\log_{10}(f_0) + b, \tag{8}$$
$$\log_{10}\left(S/B'\right) = c.\log_{10}(H_B) + d, \tag{9}$$

where a, b, c, and d are the regression coefficients. The regression coefficients are summarized in Table 2.

4.1.1 Regional site amplification factors

Figure 9 plots the average site amplification factors for sites with V_{S30} of 180, 360, and 600 m/s, respectively, where the amplifications are derived using the coefficients of Table 1 (all KiK-net data). We also show our estimate of a representative site amplification curve for the reference velocity of 760 m/s. Table 3 shows the amplifications that come from the regression of log(H/V[depth]) vs. log(V_S[depth]), evaluated at $V_S = 760$ m/s (black line in Fig. 9).

4.1.2 Additional site factor: kappa filter

The attenuation of site amplifications at high frequencies, as seen in Fig. 9, is often represented by the high-frequency attenuation operator, kappa κ (Anderson and Hough 1984). This high-frequency decay of ground motions can be modeled by multiplying the spectrum by the factor P(f):

Table 2 Regression coefficients of corrected site amplifications relative to the fundamental site frequency (a and b) and depth-to-bedrock (c and d), respectively

Frequency (Hz)	Period (s)	Fundamental frequency (f_0)		Depth-to-bedrock (H_B)	
		a	b	c	d
0.11	9.09	−0.0670	0.0157	0.0467	−0.0875
0.14	7.14	−0.0678	0.0329	0.0513	−0.0768
0.17	5.88	−0.0650	0.0418	0.0522	−0.0673
0.22	4.55	−0.0716	0.0584	0.0603	−0.0655
0.27	3.70	−0.0971	0.0860	0.0822	−0.0826
0.33	3.03	−0.1304	0.1188	0.1076	−0.1039
0.41	2.44	−0.1534	0.1464	0.1277	−0.1170
0.52	1.92	−0.1966	0.1936	0.1626	−0.1427
0.64	1.56	−0.2208	0.2272	0.1832	−0.1512
0.80	1.25	−0.2398	0.2652	0.2041	−0.1526
0.99	1.01	−0.2615	0.3142	0.2288	−0.1496
1.23	0.81	−0.2956	0.3827	0.2618	−0.1457
1.53	0.65	−0.3099	0.4472	0.2788	−0.1124
1.90	0.53	−0.3011	0.5065	0.2807	−0.0503
2.37	0.42	−0.2849	0.5747	0.2673	0.0457
2.94	0.34	−0.2534	0.6231	0.2280	0.1655
3.66	0.27	−0.1492	0.6166	0.1316	0.3506
4.55	0.22	−0.0655	0.6160	0.0796	0.4705
5.66	0.18	0.0308	0.5980	0.0120	0.6013
7.04	0.14	0.1411	0.5522	−0.0854	0.7523
8.75	0.11	0.2375	0.4801	−0.1683	0.8493
10.88	0.09	0.2731	0.3997	−0.2032	0.8370
13.53	0.07	0.2666	0.2935	−0.2277	0.7590

Fig. 9 Amplification (S/B′) for different NEHRP site classes (soft soil profile in *solid black*; stiff soil profile in *red*; and very dense soil and soft rock in *green*). The estimated amplification for a reference velocity of 760 m/s is shown in *black* (*dashed line*)
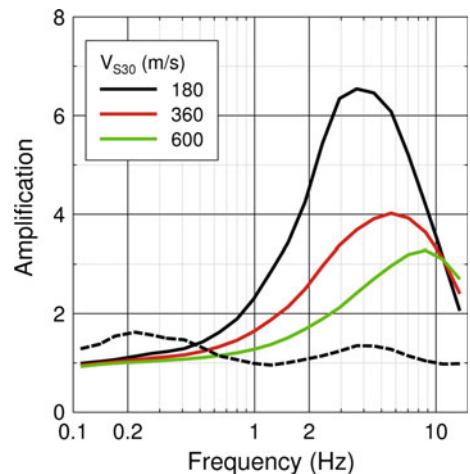
Table 3 Ratio of horizontal to vertical component of ground-motion at depth, evaluated for the reference B/C boundary site condition (V_S[depth] = 760 m/s)

Frequency (Hz)	Period (s)	H/V[depth] for V_S[depth] = 760 m/s [Regional site amplification]
0.11	9.09	1.2867
0.14	7.14	1.3798
0.17	5.88	1.5423
0.22	4.55	1.6225
0.27	3.70	1.5661
0.33	3.03	1.4982
0.41	2.44	1.4688
0.52	1.92	1.3020
0.64	1.56	1.1416
0.80	1.25	1.0644
0.99	1.01	0.9900
1.23	0.81	0.9548
1.53	0.65	1.0047
1.90	0.53	1.0716
2.37	0.42	1.1443
2.94	0.34	1.2378
3.66	0.27	1.3490
4.55	0.22	1.3419
5.66	0.18	1.2740
7.04	0.14	1.1415
8.75	0.11	1.0423
10.88	0.09	0.9765
13.53	0.07	0.9845

$$P(f) = \exp(-\pi f \kappa), \tag{10}$$

where κ is a region-dependent or site-dependent parameter. In general, kappa will increase with distance due to path effects; its zero-distance intercept, sometimes referred to as κ_0, is considered to represent path-independent near-surface attenuation of seismic waves.

After correcting ground motions from the Tohoku mainshock for regional site effects using the coefficients given in Table 1, we performed a simple regression analysis to estimate the anelastic attenuation factor, assuming a fixed geometrical spreading with slope of -1 over all distance ranges:

$$\log_{10}(FAS) = c_0 - \log_{10}(R_{eff}) + c_1 R_{cd}, \tag{11}$$

where $R_{eff} = \sqrt{R_{cd}^2 + 10^2}$ and R_{cd} is the closest-distance to the rupture surface, which is calculated based on the geometrical parameters of the background fault plane including fault length, fault width, strike, dip, and depth to the top of the fault plane (GSI 2011). Based on FAS regressions, we evaluated and plotted out the spectral shape on a log-linear plot for a

Fig. 10 *Spectral shapes* from
initial regression of FAS (Tohoku
mainshock) after site correction
in log-linear scale. The shape is
consistent for different effective
distances (R_{eff}) of 10, 20, and
50 km. The slope of the *fitted
lines* (*dashed lines*) for
frequencies > 2 Hz provides an
estimated kappa = 0.044
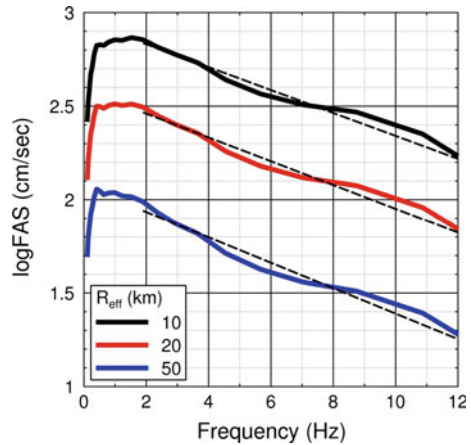
few values of near-source distances, as shown in Fig. 10. We infer $\kappa = 0.044$ from these spectral shapes.

4.1.3 Using H/V[surface] as an extra parameter to estimate site amplification function

The H/V spectral ratio has been widely used to provide a preliminary estimate of site amplification (Kanai and Tanaka 1961; Nogoshi and Igarashi 1971; Nakamura 1989). The H/V ratios on soft soil sites generally exhibit a clear, stable peak that is correlated with the fundamental resonant frequency (Ohmachi et al. 1991; Field and Jacob 1993, 1995; Lermo and Chávez-García 1994; Lachet et al. 1996; Bonnefoy-Claudet et al. 2006). However, they typically underestimate the site amplification factor (Field and Jacob 1995; Bonilla et al. 1997; Satoh et al. 2001b). Considering these findings, we explore the use of the H/V ratios as an amplification function for the KiK-net data. This will be useful for other applications where the H/V ratios are known but borehole data are not available to constrain site amplification.

We performed a linear regression using:

$$\log_{10}(Y) = a_1 . \log_{10}(V_{S30}/760) + a_2 . \log_{10}(f_0) + a_3, \tag{12}$$

in which Y is the ratio of the "true" site amplification (S/B′) to an estimate obtained as the average of H/V[surface] over many events, and f_0 is the fundamental frequency of a site as measured from its average H/V peak frequency. Figure 11 shows the performance of Eq. (12) as a predictor of site amplification; Table 4 summarizes the regression coefficients for 23 logarithmically spaced frequencies. By using the H/V ratios and V_{S30} with Eq. (12), we obtain an excellent match to the observed site transfer functions for the whole range of frequencies. Applying this new model, over all KiK-net stations, the residuals ($\log_{10}(obs) - \log_{10}(pred)$) of site amplification as a function of V_{S30} is plotted in Fig. 12. Using the combination of f_0 and V_{S30} gives near-zero average residuals for prediction of site amplification for a wide range of site classes. The advantage of this method could be significant for assessing the site effects by using a single station or in an area where a rock reference site cannot be found.

4.2 Non-linear site amplification

To this point, we have assumed linear soil behavior in assessing average site amplification. Under weak motions, the stress-strain relationship of soil is linear, i.e. stress = G × strain,
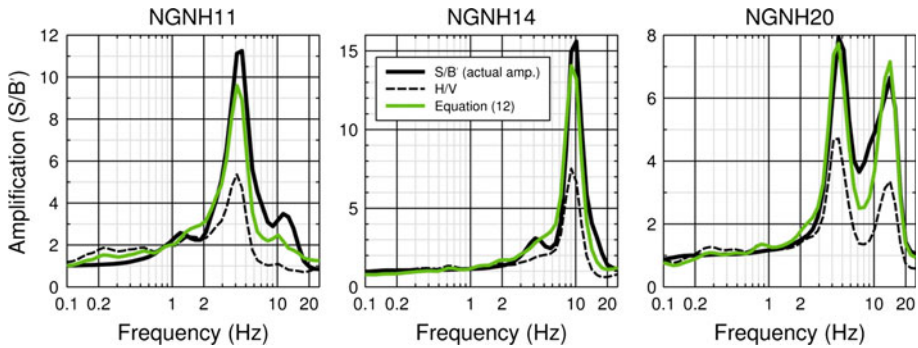
Fig. 11 Comparison of S/B′ ratios using cross-spectral ratios (*solid black line*) for sample sites (NGNH11, NGNH14, and NGNH20) with mean H/V ratios (*dashed black line*). Transfer functions are overlaid by prediction model using V_{S30} and f_0 as predictor parameters and adding H/V as an extra parameter (*green line*)

where G is the shear modulus. Under strong shaking, soil shows nonlinear and hysteretic behavior, with the effective modulus G decreasing at high strain (Beresnev and Wen 1996a). Since the shear-wave velocity is given by $V_s = \sqrt{G/\rho}$ (where ρ is density), the effective shear-wave velocity decreases as the strain increases. On the other hand, amplification decreases due to damping (loss of energy) in hysteresis. Overall, nonlinearity will result in a shift of the resonance frequency to lower values, and the reduction in amplification, as the amplitude of motions increases (Silva 1986; Beresnev and Wen 1996b; Field et al. 1997; Dimitriu et al. 2000).

Figure 13 shows the nonlinear behavior of a site subjected to strong shaking (PGA $\sim 530 \text{cm/s}^2$) during the Tohoku event. The spectral ratio of the station (MYGH04 from the KiK-net, with $V_{S30} = 850 \text{ m/s}$) is compared for the strongest part of the signal and the coda-window, noting that the shaking during the coda is a representative of weak-motion (Chin and Aki 1991). We hypothesize that the linear-elastic soil response is restored after the termination of the strong shaking portion. We have assumed that the coda window starts at the lapse time later than seven times the S-wave arrival time. If nonlinear behavior exists, it should appear as a discrepancy in site response characteristics between weak and strong motions. From Fig. 13, a clear shift of the peak amplitude frequency (fundamental frequency) to lower frequencies during the strong shaking portion of the record can be seen. Also, the amplitudes are reduced for the S-window spectral ratios in comparison with the coda-window spectral ratios. However, it should be mentioned that the coda-window does not necessarily behave in a completely linear fashion. If soil behaves nonlinearly, some residual deformation may remain, and it takes at least some time to reconsolidate to the original state (Wu et al. 2010). For Tohoku, at some sites the dissipation of pore pressure due to ground shaking might have taken a long time because of the long duration of shaking. Extensive liquefaction effects are hypothesized to be related to the number of cycles that soil underwent during the Tohoku event (Bhattacharya et al. 2011).

By contrast to the nonlinear behavior noted in Fig. 13, we observe linear behavior in Fig. 14, which shows similar amplification of S-window and coda-window for TCGH16. V_{S30} for this site is 213 m/s and the borehole is at the depth of 112 m, in a layer with shear-wave velocity 680 m/s. The ground-motions reached PGA of 1, 197 cm/s^2 in the EW component on the surface, and the PGA of the vertical component at the borehole level is 137 cm/s^2; this is above a common threshold level of $\sim 100 \text{cm/s}^2$ often cited for nonlinearity for surface ground-motions (Beresnev and Wen 1996b).

**Table 4** Regression coefficients for predicting site amplification (S/B′) using Eq. (12)

Frequency (Hz)	Period (s)	a_1	a_2	a_3
0.11	9.09	0.148	−0.0430	0.001
0.14	7.14	0.143	−0.0334	−0.015
0.17	5.88	0.155	−0.0314	−0.025
0.22	4.55	0.122	−0.0356	−0.028
0.27	3.70	0.103	−0.0317	−0.029
0.33	3.03	0.093	−0.0377	−0.023
0.41	2.44	0.083	−0.0401	−0.014
0.52	1.92	0.075	−0.0646	0.018
0.64	1.56	0.057	−0.0929	0.051
0.80	1.25	0.044	−0.0862	0.057
0.99	1.01	0.020	−0.0842	0.065
1.23	0.81	−0.012	−0.1122	0.099
1.53	0.65	−0.028	−0.1211	0.131
1.90	0.53	−0.087	−0.1345	0.166
2.37	0.42	−0.180	−0.1287	0.179
2.94	0.34	−0.214	−0.1344	0.208
3.66	0.27	−0.260	−0.1328	0.229
4.55	0.22	−0.358	−0.1445	0.253
5.66	0.18	−0.381	−0.1534	0.284
7.04	0.14	−0.372	−0.1343	0.288
8.75	0.11	−0.323	−0.1053	0.302
10.88	0.09	−0.260	−0.0608	0.312
13.53	0.07	−0.155	−0.0171	0.314
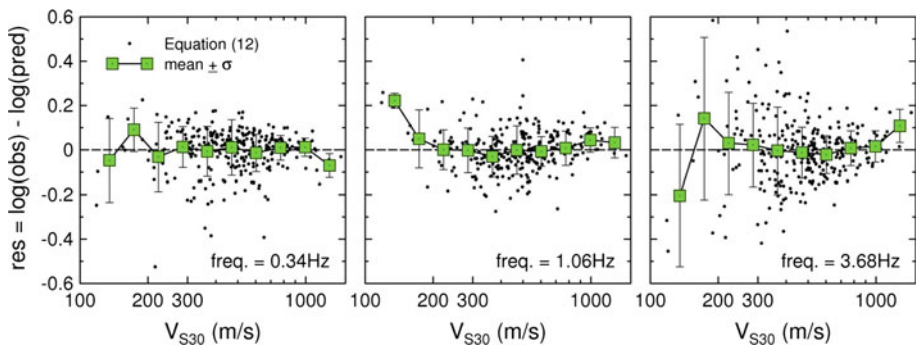
Fig. 12 Residuals of predicting corrected observed amplifications at different site classes (varying V_{S30}) using f_0, depth-to-bedrock, and H/V as an extra parameter [Eq. (12)]. Bars are indicating $\pm 1\sigma$ around the mean

4.2.1 Time-frequency analysis of borehole data to assess nonlinearity

We apply a moving-window method of Sawazaki et al. (2006; 2009) and Wu et al. (2009; 2011) to detect the PGA threshold of nonlinearity for each station. This technique uses Welch's
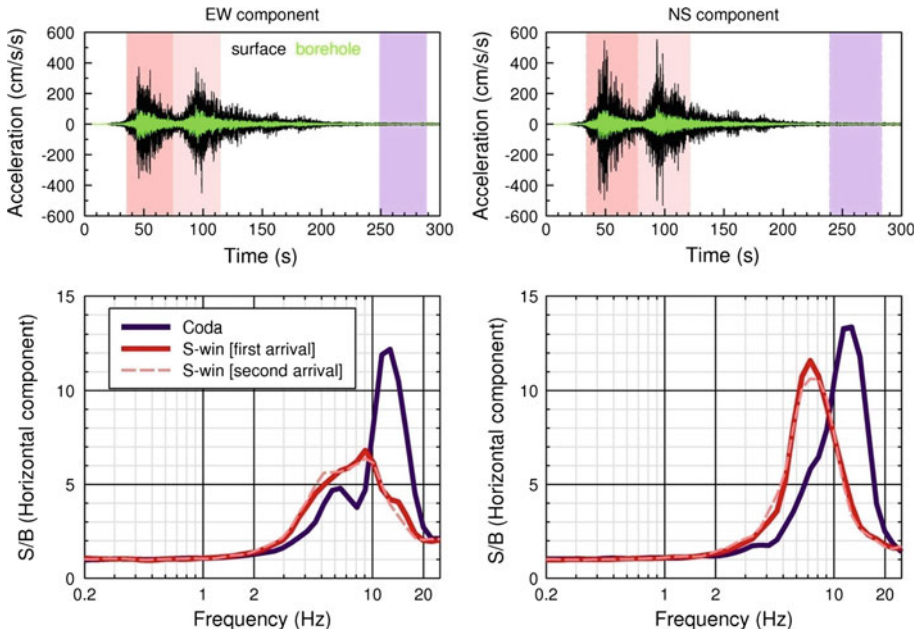
Fig. 13 Amplification (S/B) of the East–West (EW) and North–South (NS) components at MYGH04 for the S-window of the first arrival (*tick solid red*), S-window of the second arrivals (*dashed light red*), and coda-window (*blue*)
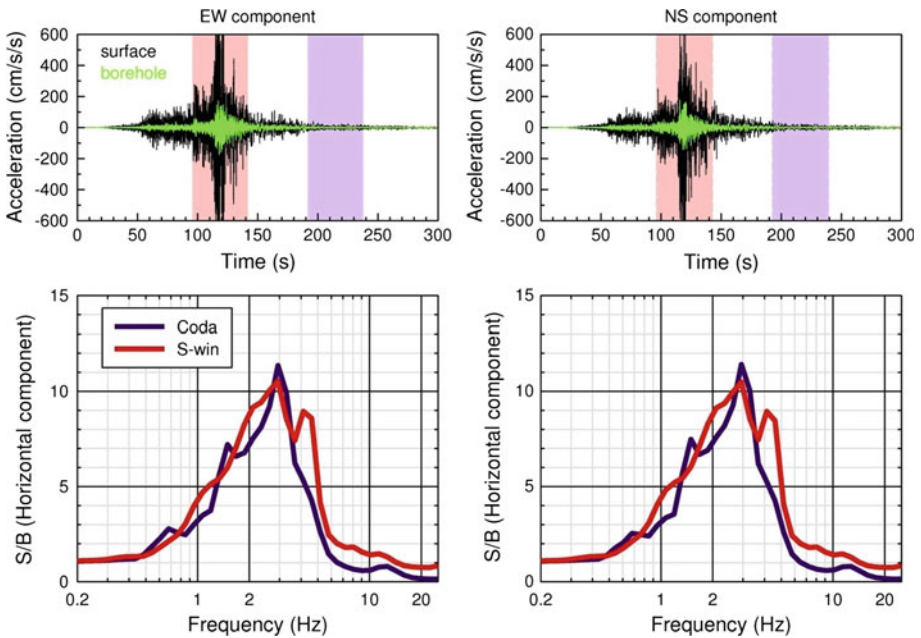
Fig. 14 Amplification (S/B) of the East-West (EW) and North–South (NS) components at TCGH16 for the S-window (*red*) and coda-window (*blue*)

periodogram method of spectral estimation. The short-time Fourier transform (STFT) of a moving window is calculated for both surface and borehole time series. Then, the spectra are plotted versus evolutionary time. This way, a decrease of fundamental frequency and amplitude due to the nonlinear behavior of a site can be detected within the strong part of the signal, relative to the coda window and background noise (representing weak motions). A sample application of the technique is depicted in Fig. 15.

In our implementation, we used a moving window with a length of 6 s to examine all Tohoku waveforms recorded by the surface and borehole stations. Successive windows have 67 % overlap (windows are moved forward by 2 s intervals). The employed 6 s window appears to offer a good balance between temporal resolution and stability (Wu et al. 2009, 2010). We remove any linear trend and apply a 5 % cosine-taper to both ends of each window, and compute the FAS of the two horizontal components. The spectra is then smoothed using a Konno–Ohmachi window ($b = 20$; where b is the bandwidth coefficient). The spectral ratios (S/B′) are obtained by dividing the geometric mean of horizontal FAS spectra of a surface station by the corresponding spectra of a borehole station, tabulated for 50 frequencies logarithmically spaced between 0.1 and 25 Hz; we extended the upper-bound frequency as the S/B′ ratio is a dimensionless quantity and instrument correction can be ignored. Estimating a threshold for nonlinear behavior, we plot the S/B′ ratios as a function of sorted PGA values obtained from each record at the borehole level. PGA values are binned into 100 classes.

Figure 16 illustrates the changes of S/B′ relative to PGA for MYGH04. Note the reduction in the fundamental frequency and the amplification with increasing PGA. The threshold for
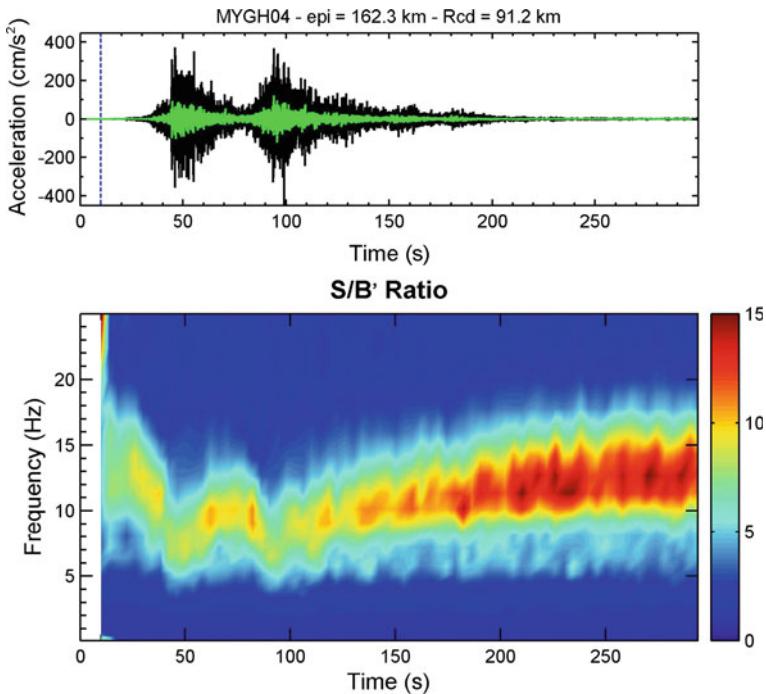

Fig. 15 Temporal evolution of S/B′ for the MYGH04 station. The drop of amplitude and shifting of the fundamental frequency to lower-frequencies during strong shaking can be seen clearly in this figure
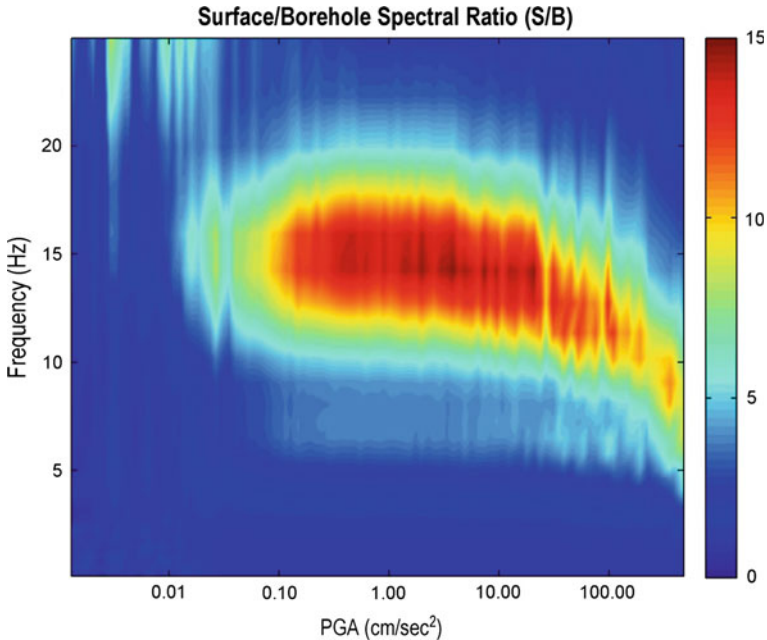
Fig. 16 Spectral ratios versus recorded PGA for MYGH04. The threshold ground motion for nonlinear behavior is PGA[surface] $\sim 25\text{cm/s}^2$

nonlinearity at this station is $\sim$25 cm/s^2. For this station, soil response at the surface starts to deviate from linear response at 25 cm/s^2, becoming significant at 100cm/s^2. MYGH04 has a 4 m thick soil layer with shear-wave velocity of 220 m/s over a 10 m thick of very stiff soil or soft rock layer with a shear-wave velocity of 960 m/s. For this site, it may take a large surface acceleration before the soil develops strong nonlinear response: the ratio of inertial force (i.e. accelerations times mass) over the yielding shear-stress of the soil above the base can be quite small even when the acceleration is large, due to the small thickness of the soil layer (J. Zhao, personal communication, 2012). The threshold values for nonlinearity based on PGA[surface] and PGA[borehole] are estimated and tabulated for 49 KiK-net stations in "Appendix 2".

To examine the relative degree of nonlinearity during the Tohoku mainshock, in comparison to that exhibited during smaller earthquakes, we calculate the average amplification (S/B$'$) at each station over all events (A_{ref}) and the frequency of that peak (f_{ref}). The same procedure is also applied for just the Tohoku mainshock ground motions. In this case, the maximum amplitude is called A_{MS} and the fundamental frequency is called f_{MS}. We consider stations that show a clear-single peak (with amplitude > 2) in the H/V ratios at the surface (or S/B$'$ ratio). In total, 225 out of 475 stations passed these criteria and among them only 42 stations showed nonlinear behavior (shifting of the fundamental frequency to lower frequencies, and a decrease in amplitude). To quantify the degree of nonlinearity for these 42 stations, we plot the ratio $A_{\text{MS}}/A_{\text{ref}}$ and $f_{\text{MS}}/f_{\text{ref}}$ as a function of PGA$_{\text{ref}}$, the predicted median PGA by the Tohoku regression Eq. (13) (derived below), for V$_{S30} = 760$ m/s (reference), in Fig. 17 (values for other sites, not identified as being nonlinear, as shown in the background). It is interesting that nonlinear effects are seen for all soil types. Probably this is because the NEHRP C sites are typically soft shallow soil over rock. The plots
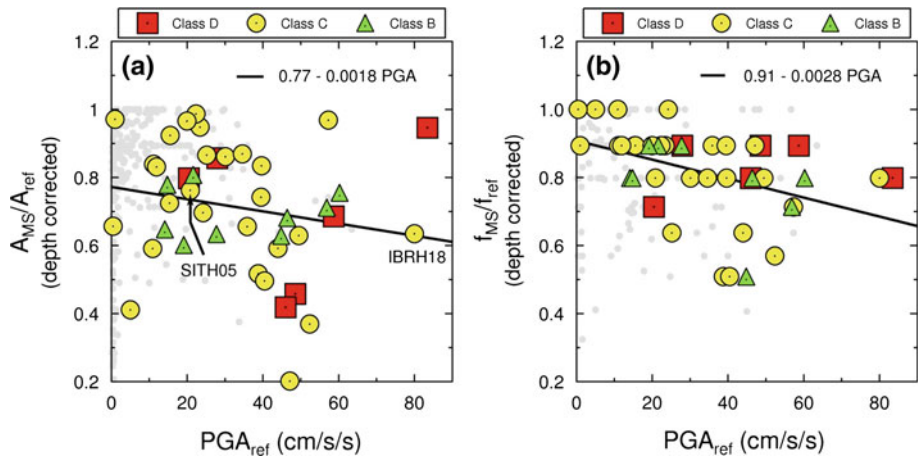
Fig. 17 Nonlinearity symptoms: decrease in the predominant frequency (f_{MS}/f_{ref}) and/or amplification amplitude (A_{MS}/A_{ref}) as a function of PGA_{ref} (predicted PGA for $V_{S30} = 760$ m/s). NEHRP site classes are shown with different colors (**a** and **b**) and *trend lines* are shown as solid black lines. *Grey dots* in background show values for sites that did not exhibit nonlinearity symptoms

show that there is a clear, steady trend of increasing nonlinearity with increasing PGA. We fit a linear trend line (for the sites showing nonlinearity) and obtain the significance of slope and intercept for A_{MS}/A_{ref} and f_{MS}/f_{ref} ratios. The p-value of the 2-tailed t-test for the slope (Fig. 17a) is 0.22, which is significantly different from 0 at the 95 % confidence level. The standard error (SE) on the slope for A_{MS}/A_{ref} is 0.0014. For the f_{MS}/f_{ref} ratio, the p-value of the slope is 0.0048, which indicates significant difference from 0 (with $SE = 9.3 \times 10^{-4}$).

In summary, we found some localized nonlinear soil behavior (such as stations MYGH04 and IBRH18), and the degree of nonlinearity increases with the intensity of shaking as would be expected (Fig. 17). However, nonlinearity was not a pervasive phenomenon during the Tohoku event, with only a small fraction of the sites showing significant changes in amplification and its peak frequency. On the other hand, it should be mentioned that there are many cases of liquefaction-related damage during the Tohoku earthquake, and that some nonlinearity was also observed at the K-NET sites (Tokimatsu et al. 2011).

5 Overall characteristics of Tohoku ground motions

Having evaluated site amplification for the Tohoku motions, we can now examine what the underlying motions would be without the site effects. We fit the Tohoku motions to:

$$\log_{10}(Y) + \log_{10}(R_{eff}) - site_{factor} = c_0 + c_1.F.R_{cd} + c_2.B.R_{cd} \qquad (13)$$

For stations in the forearc region, F = 1 and B = 0, otherwise (for backarc stations) F = 0 and B = 1 (Ghofrani and Atkinson 2011). The $site_{factor}$ is $m.\log(V_{S30}/V_{ref}) + b$ using coefficients in Table 1. The regression coefficients are given for both FAS and pseudo-spectral acceleration (PSA) in Table 5.

A comparison between the event-specific Tohoku prediction equation and the motions prescribed by regional GMPEs for Japan (Zhao et al. 2006b; Kanno et al. 2006; Atkinson and

Table 5 Regression coefficients for FAS and PSA (geometric mean of horizontal components)

Frequency (Hz)	Period (s)	FAS (cm/s)			PSA (cm/s^2)		
		c_0	c_1	c_2	c_0	c_1	c_2
0.11	9.09	3.4456	−0.0002	−0.0005	3.1224	−0.0001	−0.0005
0.14	7.14	3.5413	–	−0.0005	3.2570	–	−0.0005
0.17	5.88	3.5787	–	−0.0006	3.3658	–	−0.0006
0.22	4.55	3.6569	−0.0003	−0.0008	3.5190	−0.0001	−0.0008
0.27	3.70	3.7003	−0.0002	−0.0009	3.6427	−0.0002	−0.0009
0.33	3.03	3.7444	−0.0002	−0.0011	3.7505	−0.0002	−0.0010
0.41	2.44	3.7880	−0.0004	−0.0012	3.8629	−0.0003	−0.0011
0.52	1.92	3.8023	−0.0005	−0.0013	3.9604	−0.0005	−0.0013
0.64	1.56	3.8171	−0.0008	−0.0016	4.0347	−0.0007	−0.0015
0.80	1.25	3.8331	−0.0009	−0.0018	4.1204	−0.0008	−0.0017
0.99	1.01	3.8313	−0.0010	−0.0020	4.1890	−0.0009	−0.0019
1.23	0.81	3.8248	−0.0011	−0.0022	4.2362	−0.0009	−0.0020
1.53	0.65	3.7907	−0.0011	−0.0024	4.2714	−0.0010	−0.0022
1.90	0.53	3.7632	−0.0013	−0.0026	4.3027	−0.0011	−0.0024
2.37	0.42	3.7127	−0.0015	−0.0029	4.3138	−0.0012	−0.0025
2.94	0.34	3.6796	−0.0016	−0.0031	4.3263	−0.0013	−0.0027
3.66	0.27	3.6362	−0.0017	−0.0034	4.3306	−0.0013	−0.0028
4.55	0.22	3.5738	−0.0017	−0.0036	4.3269	−0.0013	−0.0028
5.66	0.18	3.4999	−0.0017	−0.0037	4.3150	−0.0012	−0.0029
7.04	0.14	3.3856	−0.0015	−0.0037	4.3025	−0.0011	−0.0028
8.75	0.11	3.2471	−0.0014	−0.0037	4.2814	−0.0010	−0.0028
10.88	0.09	3.0018	−0.0011	−0.0035	4.2322	−0.0009	−0.0027
13.53	0.07	2.6419	−0.0008	−0.0032	4.2188	−0.0008	−0.0025

Macias 2009) is shown in Fig. 18. In this figure, AM09 is in fact a GMPE for Cascadia which is adjusted for Japan by multiplying the Cascadia motions by the ratio of Japan/Cascadia site factors, as given by Macias et al. (2008) and Atkinson and Macias (2009), respectively. The observed PSA values are corrected for site amplification using coefficients from Table 1, before comparison with GMPEs for a reference condition of B/C. The Zae06 (Zhao et al. 2006b) and Kan06 (Kanno et al. 2006) GMPEs are over-predicting Tohoku ground motions at 1 Hz, while AM09 (Atkinson and Macias 2009) is similar to the new Tohoku equation for the back-arc stations. The magnitude scaling for very large megathrust events is not empirically-constrained, and thus extrapolation of empirical GMPEs may cause unknown biases. For example, the over-prediction of ground-motions using Zae06 and Kan06 could be the result of inadequacy of the magnitude squared term for magnitude scaling of subduction interface earthquakes in their relations (Zhao and Xu 2012a). The relatively-good agreement of the site-corrected data with the AM09 predictions, while encouraging, should be interpreted with caution as this result pertains to a single event, at a specific magnitude. It is clear from Fig.18 that the attenuation (slope and curvature) of single Q-factor GMPEs is controlled mostly by the back-arc stations.
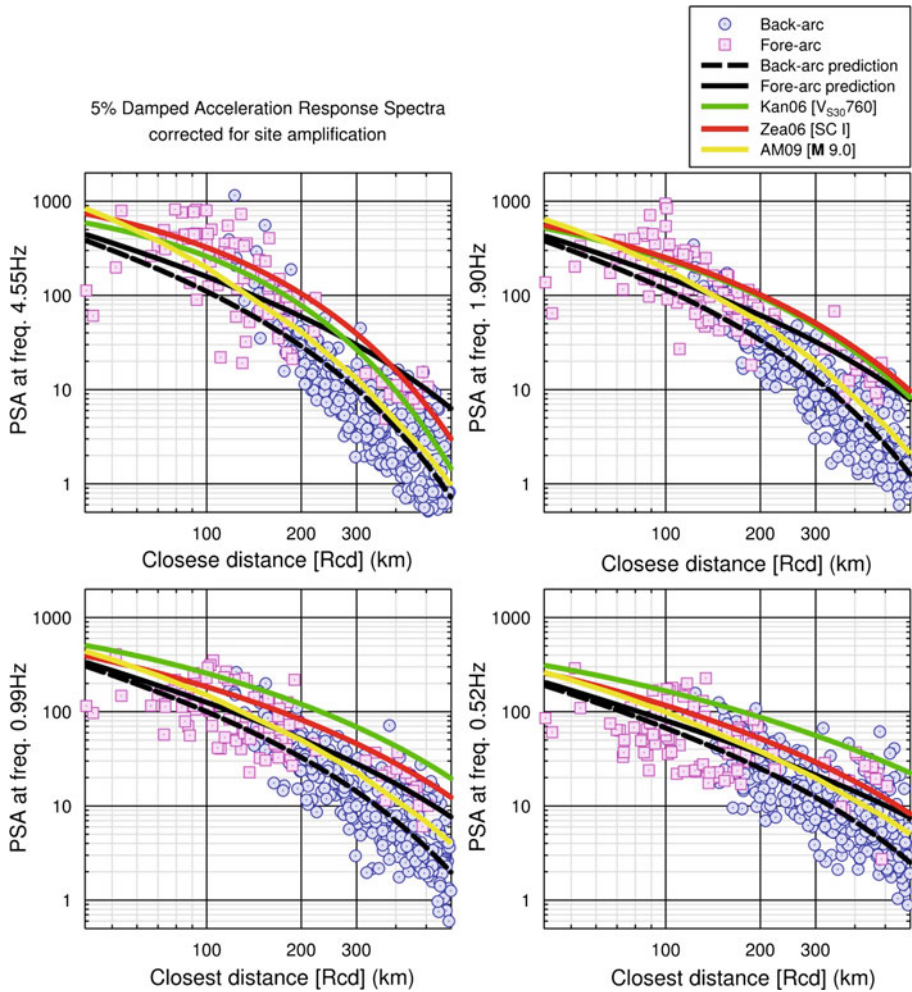
Fig. 18 Comparing event-specific prediction equation for the site corrected Tohoku ground-motions (B/C) with other GMPEs (Kan06 = Kanno et al. 2006; Zea06 = Zhao et al. 2006b; AM09 = Atkinson and Macias 2009) at four frequencies. *Fore-arc* stations are shown with *blue circles* and *back-arc* stations are in *magenta*

6 Conclusions

The **M**9.0 2011 Tohoku earthquake has provided important new quantitative information on site response that is invaluable in refining seismic hazard analysis and mitigation efforts. Conclusions from our study of site effects are as follows:

1. Site amplification effects in Japan are very large at f > 2 Hz, with amplification factors of 4 to 8, even for relatively strong shaking. At high frequencies, median peak ground accelerations from the Tohoku event were near 300 cm/s^2 (∼0.30g) at 100 km, for the NEHRP C sites, largely due to high-frequency site effects. The site amplifications were much greater than those adopted in standard building code based on the NEHRP site class. In part, the large amplitudes at high frequencies are due to the prevalence of shallow soil

conditions over a harder layer in Japan; this is especially applicable for the KiK-net sites. Accounting for site amplification is critical to interpretation of motions.

2. Analyzing spectral ratios of motions recorded on the surface to those at depth in boreholes are a good way of obtaining site response at stations, but should be corrected for the depth effect (interference of up-going and down-going waves). A cross-spectral ratio technique for correcting the depth effect of the surface-to-borehole ratios is effective.

3. We estimated the frequency-dependent site amplification factors that relate the recorded motions to equivalent values for the B/C boundary site conditions. The regression coefficients (amplification factors) are derived for the Tohoku event and for all KiK-net data ($\mathbf{M} \geq 5.5$; 1998–2009) for the frequency range of 0.1–15 Hz (Table 1).

4. We developed empirical relationships between parameters that characterize site amplification, depth-to-bedrock and fundamental site frequency. It is interesting that V_{S30} is a good proxy to estimate the natural frequency of a site. Furthermore, the fundamental frequency inferred from H/V matches well with that derived from the theoretical relation ($f_0 = V_S/4H$).

5. Nonlinear site response was not pervasive during the 2011 $\mathbf{M}9.0$ Tohoku earthquake at the KiK-net stations. No specific dependence of nonlinearity on the site properties (e.g. V_{S30}) was observed. This may be because V_{S30} is not providing a good measure of soil stiffness in Japan, as the stiffer sites are mostly just shallow soft soil.

6. We can obtain an excellent match to the observed site transfer functions for the whole range of frequencies by using H/V and V_{S30}, with Eq. (12). Using the combination of f_0 and V_{S30} gives near-zero average residuals for prediction of site amplification for a wide range of site classes. The advantage of this method could be significant for assessing the site effects by using a single station or in an area where a rock reference site cannot be found.

7. Generic GMPEs developed for subduction regions appear to under-estimate the Tohoku motions if soil amplification effects are not removed. However, once site effects are taken into account the agreement is improved.

7 Appendix 1: List of notations

f_0: fundamental resonance frequency
FAS: Fourier amplitude spectrum of acceleration
FAS[surface] and FAS[depth]: FAS at the surface and bottom of borehole, respectively.
f_{d1}: destructive interference frequency
GMPE: ground motion prediction equation
H/V: horizontal-to-vertical spectral ratio
H/V[surface] and H/V[depth]: H/V at surface and at the bottom of the borehole, respectively.
$\mathbf{M}$: Moment magnitude
PGA: peak ground acceleration

PGA_{ref}: predicted median PGA by the Tohoku regression equation for $V_{S30} = 760$ m/s (reference)

PSA: Pseudo- acceleration response spectrum, 5 % damped

SSR: standard spectral ratios (ratio of the motions recorded on a soil site to those recorded on a nearby rock site)

S/B: surface-to-borehole spectral ratio ("site amplification")

S/B' and S/B'(vert): S/B corrected for depth effect for horizontal and vertical component, respectively

V_S[depth]: shear-wave velocity at the bottom of the borehole

V_{S30}: time-averaged shear-wave velocity over top 30 m

8 Appendix 2: Nonlinearity thresholds for the selected KiK-NET stations

Following table contains: station code, station latitude and longitude, V_{S30}, total number of events recorded by each station, PGA[depth] and corresponding PGA[surface] for vertical components, maximum and minimum moment magnitude, epicentral distance, and depth of events, respectively.

Station code	lat (°)	lon (°)	V_{S30}(m/s)	# events†	PGA (cm/s²)*		M		Distance (km)		Depth (km)	
					UD1	UD2	min	max	min	max	min	max
AICH10	34.997	137.627	504.86	21	7.4	12.2	5.5	7.4	82.5	1120.9	11.0	598.0
ABSH12	43.854	144.461	268.54	101	2.1	4.1	5.5	8.2	50.3	1712.6	0.0	589.0
AKTH05	39.069	140.322	829.46	54	19.2	153.6	5.6	7.2	8.1	893.3	0.0	589.0
AKTH16	39.542	140.352	375.00	99	9.1	11.8	5.5	8.2	56.8	1454.3	0.0	589.0
AKTH17	39.555	140.615	288.82	91	8.5	36.0	5.5	8.2	58.7	1436.0	0.0	589.0
AKTH19	39.189	140.474	287.96	62	7.7	11.0	5.5	8.2	26.4	1460.8	0.0	589.0
AOMH01	41.525	140.916	301.99	105	4.6	9.0	5.5	8.2	28.9	1410.5	0.0	589.0
AOMH02	41.402	140.860	872.48	22	4.6	9.0	5.6	7.2	122.0	810.4	0.0	589.0
AOMH12	40.582	141.158	281.00	135	12.8	58.0	5.5	8.2	103.3	1328.7	0.0	589.0
FKSH04	37.448	139.816	245.88	77	6.4	17.8	5.5	8.2	69.2	1748.6	0.0	589.0
FKSH10	37.159	140.096	487.02	112	7.6	19.0	5.5	8.2	91.5	1712.3	0.0	589.0
IBRH12	36.834	140.322	485.71	89	5.7	16.5	5.5	8.2	76.1	1663.9	0.0	487.0
IBRH13	36.792	140.578	335.37	88	7.4	22.1	5.5	8.2	57.7	1664.9	0.0	501.0
IBRH15	36.554	140.305	450.40	92	7.4	21.7	5.5	8.2	66.0	1688.0	0.0	501.0
IBRH16	36.637	140.401	626.15	86	7.4	21.0	5.5	8.2	64.3	1675.3	0.0	501.0
IWTH02	39.822	141.386	389.57	119	12.1	150.9	5.5	8.2	24.0	1366.4	0.0	589.0
IWTH08	40.266	141.787	304.52	76	8.7	43.5	5.5	8.2	54.4	1308.6	0.0	589.0
IWTH14	39.741	141.912	816.31	102	3.5	22.9	5.5	8.2	20.6	1338.3	0.0	589.0
IWTH22	39.331	141.305	532.13	103	7.6	25.2	5.5	8.2	7.8	1407.5	0.0	589.0
IWTH23	39.271	141.827	922.89	125	8.1	26.2	5.5	8.2	50.1	1378.7	0.0	589.0
IWTH26	38.966	141.005	371.06	131	8.3	31.9	5.5	8.2	9.8	1899.3	0.0	589.0
KOCH05	33.644	133.147	1072.16	17	7.1	25.9	5.5	7.4	66.7	597.8	8.0	528.0
KSRH02	43.112	144.127	219.14	111	6.9	10.8	5.5	8.2	75.6	1265.5	0.0	589.0

Station code	lat ($^\circ$)	lon ($^\circ$)	V_{S30} (m/s)	# events[†]	PGA (cm/s^2) *		M		Distance (km)		Depth (km)	
					UD1	UD2	min	max	min	max	min	max
KSRH03	43.382	144.632	249.76	117	5.2	24.1	5.5	8.2	28.6	1312.7	0.0	589.0
KSRH04	43.211	144.684	189.19	118	4.0	11.7	5.5	8.2	40.9	1299.0	0.0	589.0
KSRH05	43.253	144.238	388.89	110	6.1	21.9	5.5	8.2	63.1	1283.6	0.0	589.0
KSRH06	43.218	144.433	326.19	109	5.6	23.2	5.5	8.2	52.8	1288.6	0.0	589.0
KSRH07	43.133	144.331	204.10	118	7.6	35.8	5.5	8.2	62.0	1276.3	0.0	507.0
KSRH09	42.983	143.988	230.23	122	13.1	28.2	5.5	8.2	65.4	1247.4	0.0	589.0
MYGH04	38.783	141.329	849.83	116	6.9	31.4	5.5	8.2	30.7	1447.2	0.0	589.0
MYGH05	38.576	140.784	305.33	106	3.6	8.6	5.5	8.2	37.1	1497.4	0.0	589.0
MYGH09	38.006	140.606	358.25	127	9.0	21.6	5.5	8.2	66.3	1797.9	0.0	589.0
MYGH10	37.938	140.896	347.54	145	7.4	18.0	5.5	8.2	57.0	1787.0	0.0	589.0
NIGH04	38.128	139.546	392.08	93	15.7	31.9	5.5	8.2	93.4	1827.5	0.0	589.0
NIGH06	37.650	139.071	336.14	70	8.9	19.5	5.5	8.0	28.8	1784.7	0.0	589.0
NIGH09	37.536	139.131	462.93	62	7.8	15.8	5.5	8.0	18.1	1032.0	0.0	589.0
NMRH01	43.783	145.029	437.57	104	13.2	26.1	5.5	8.2	28.5	1367.4	0.0	589.0
NMRH05	43.388	144.806	208.98	107	5.6	21.4	5.5	8.2	19.0	1320.8	0.0	501.0
OITH01	33.409	131.035	865.38	5	6.2	21.4	5.6	7.3	141.0	296.9	11.0	51.0
OITH03	33.470	131.688	486.01	11	6.2	21.7	5.5	7.0	45.9	461.9	9.0	146.0
OITH06	32.969	131.401	711.94	14	6.1	22.1	5.5	7.4	17.9	535.3	9.0	146.0
OITH11	33.281	131.214	458.53	5	6.2	21.7	5.7	7.0	96.3	2024.2	9.0	496.0
OKYH01	34.504	133.893	240.85	13	10.7	40.7	5.5	7.4	99.1	516.9	9.0	340.0
OKYH04	34.640	133.689	360.16	21	7.3	26.3	5.5	7.4	73.8	865.8	8.0	528.0
OKYH05	34.865	133.855	607.92	18	8.1	32.9	5.5	7.4	64.9	649.1	8.0	350.0
OKYH06	34.672	133.531	549.74	17	13.7	51.0	5.5	7.4	62.2	619.1	8.0	350.0

Station code	lat (°)	lon (°)	V_{S30}(m/s)	# events[†]	PGA (cm/s^2)*		M		Distance (km)		Depth (km)	
					UD1	UD2	min	max	min	max	min	max
OSKH01	34.394	135.286	500.00	14	10.8	37.3	5.5	7.4	98.0	568.2	9.0	340.0
TKCH05	43.119	143.622	337.28	100	13.5	35.2	5.5	8.2	87.8	1245.3	0.0	589.0
TKCH08	42.484	143.156	353.21	108	10.5	32.4	5.5	8.2	19.0	1165.3	0.0	589.0

[†] The total number of events recorded by each station during 1998 to 2009 * UD1 and UD2 are PGA[borehole] and PGA[surface], respectively

References

Abercrombie RE (1997) Near-surface attenuation and site effects from comparison of surface and deep borehole recording. Bull Seism Soc Am 87:731–744

Aguirre J, Irikura K (1997) Nonlinearity, liquefaction, and velocity variation of soft soil layers in Port Island, Kobe, during the Hyogoken-Nanbu earthquake. Bull Seism Soc Am 87:1244–1258

Anderson JG, Hough SE (1984) A model for the shape of the Fourier amplitude spectrum of acceleration at high frequencies. Bull Seism Soc Am 74:1969–1994

Andrews DJ (1986) Objective determination of source parameters and similarity of earthquakes of different size. Earthquake source mechanics, 37:259–267

Aoi S, Kunugi T, Suzuki W, Morikawa N, Nakamura H, Pulido N, Asano Y, Shiomi K, Fujiwara H (2011) Characteristics of the 2011 Tohoku-oki earthquake revealed by the seismograph networks operated by NIED. Japan Geoscience Union Meeting (2011) (May 22–27, 2011 at Makuhari. Chiba, Japan)

Assimaki D, Li W, Steidl J, Tsuda K (2008) Site amplification and attenuation via downhole array seismogram inversion: a comparative study of the 2003 Miyagi-Oki aftershock sequence. Bull Seism Soc Am 98: 301–330

Atakan K (1995) A review of the type of data and techniques used in the empirical estimation of local site response. In: Proceedings of the fifth international conference on seismic zonation, Nice, France, OuestÉditions, Presses Académiques, vol II, pp 1451–1460

Atkinson GM, Macias M (2009) Predicted ground motions for great interface earthquakes in the Cascadia subduction zone. Bull Seism Soc Am 99:1552–1578

Bard P-Y (1994) Effects of surface geology on ground motion: Recent results and remaining issues. In: Proceedings of the 10th European conference on earthquake engineering, vol 1. Vienna, Austria, pp 305–323 Aug 28–Sept 2

Bendat JS, Piersol AG (2006) Engineering applications of correlation and spectral analysis. Wiley, New York

Beresnev IA, Wen K-L (1996a) The accuracy of soil response estimates using soil-to-rock spectral ratios. Bull Seism Soc Am 86:519–523

Beresnev IA, Wen K-L (1996b) Nonlinear soil response—a reality? Bull Seism Soc Am 86:1964–1978

Bhattacharya S, Hyodo M, Goda K, Tazoh T, Taylor CA (2011) Liquefaction of soil in the Tokyo Bayarea from the 2011 Tohoku (Japan) earthquake. Soil Dyn Earthq Eng 31:1618–1628

Boatwright J, Fletcher JB, Fumal TE (1991) A general inversion scheme for source, site and propagation characteristics using multiply recorded sets of moderate-sized earthquakes. Bull Seism Soc Am 81: 1754–1782

Bonilla LF, Steidl JH, Lindley GT, Tumarkin AG, Archuleta RJ (1997) Site amplification in the San Fernando Valley, California: variability of site-effect estimation using the S-wave, coda, and H/V methods. Bull Seism Soc Am 87:710–730

Bonnefoy-Claudet S, Cornou C, Bard P-Y, Cotton F, Moczo P, Kristek J, Fah D (2006) H/V ratio: a tool for site effects evaluation. Results from 1-D noise simulations. Geophys. J. Int. 167:827–837

Boore DM, Joyner WB (1997) Site amplification for generic rock sites. Bull Seism Soc Am 87:327–341

Boore DM, Thompson EM, Cadet H (2011) Regional correlations of V_{S30} and velocities averaged over depths less than and greater than 30 meters. Bull Seism Soc Am 101:3046–3059

Borcherdt RD (1970) Effects of local geology on ground motion near San Francisco Bay. Bull Seism Soc Am 60:29–61

Borcherdt RD (1992) Simplified site classes and empirical amplification factors for site-dependent code provisions, NCEER, SEAOC, BSSC workshop on site response during earthquakes and seismic code provisions Proceedings, University Southern California, Los Angeles, CA, Nov 18–20, 1992

Borcherdt RD (1994) Estimates of site-dependent response spectra for design (methodology and justification). Earthquake Spectra, EERI 10:617–653

Borcherdt RD, Wentworth CW (1995) Strong-ground motion generated by the Northridge earthquake of January 17, 1994, Implications for seismic design coefficients and seismic zonation. In: Fifth international conference on Seismic Zonation Proceedings, vol II. Nice, France, pp 964–971

Cadet H, Bard P-Y, Rodriguez-Marek A (2012) Site effect assessment using KiK-net data: Part 1. A simple correction procedure for surface/downhole spectral ratios. Bull Earthq Eng 10(2):421–448

Chin BH, Aki K (1991) Simultaneous study of the source, path, and site effects on strong ground motion during the 1989 Loma Prieta earthquake: a preliminary result on pervasive nonlinear site effects. Bull Seism Soc Am 81:1859–1884

Dimitriu P, Theodulidis N, Bard P-Y (2000) Evidence of nonlinear site response in HVSR from SMART1 (Taiwan) data. Soil Dyn Earthq Eng 20:155–165

Dobry R, Borcherdt R, Crouse C, Idriss I, Joyner W, Martin G, Power M, Rinne E, Seed R (2000) New site coefficients and site classification system used in recent building seismic code provisions. Earthq Spectra 16:41–67

Field EH (1996) Spectral amplification in a sediment-filled valley exhibiting clear basin-edge induced waves. Bull Seism Soc Am 86:991–1005

Field EH, Jacob KH, Hough SE (1992) Earthquake site response estimation: a weak-motion case study. Bull Seism Soc Am 82:2283–2307

Field EH, Jacob KH (1993) The theoretical response of sedimentary layers to ambient seismic noise. Geophys Res Lett 20(24):2925–2928

Field EH, Jacob KH (1995) A comparison and test of various site-response estimation techniques, including three that are not reference site dependent. Bull Seism Soc Am 85:1127–1143

Field EH, Johnson PA, Beresnev IA, Zeng Y (1997) Nonlinear ground-motion amplification by sediments during the 1994 Northridge earthquake. Nature 390:599–602

Fukushima Y, Bonilla LF, Scotti O, Douglas J (2007) Site classification using horizontal- to-vertical response spectral ratios and its impact when deriving empirical ground motion prediction equations. J Earthq Eng 11:712–724

Geospatial Information Authority (GSI) of Japan (2011). The 2011 off the Pacific coast of Tohoku earthquake: crustal deformation and fault model. http://www.gsi.go.jp/cais/topic110422-index-e.html

Ghofrani H, Atkinson GM (2011) Fore-arc versus back-arc attenuation of earthquake ground motion. Bull Seism Soc Am 101:3032–3045

Hartzell S, Leeds A, Frankel A, Michael J (1996) Site response for urban Los Angeles using aftershocks of the Northridge earthquake. Bull Seism Soc Am 86:S168–S192

Hartzell SH (1992) Site response estimation from earthquake data. Bull Seism Soc Am 82:2308–2327

Haskell NA (1960) Crustal reflection of plane SH waves. J Geophys Res 65:4147–4150

Iai S, Morita T, Kameoka T, Matsunaga Y, Abiko K (1995) Response of a dense sand deposit during 1993 Kushiro-Oki Earthquake. Soils Found 35:115–131

Kanai K, Tanaka T (1961) On microtremors VIII. Bull Earthq Res Inst 39:97–114

Kanno T, Narita A, Morikawa N, Fujiwara H, Fukushima Y (2006) A new attenuation relation for strong ground motion in Japan based on recorded data. Bull Seism Soc Am 96:879–897

Kato K, Aki K, Takemura M (1995) Site amplification from coda waves: validation and application to S-wave site response. Bull Seism Soc Am 85:467–477

Kinoshita S (1992) Local characteristic of the f_{max} of bedrock motion in the Tokyo metropolitan area, Japan. J Phys Earth 40:487–515

Kitagawa Y, Okawa I, Kashima T (1992) Dense array observation and analyses of dense strong ground motions at sites with different geological conditions in Sendai. Proceedings of the international symposium on the effects of surface geology on seismic motion, Odawara vol 1, pp 311–316

Konno K, Ohmachi T (1998) Ground motion characteristics estimated from spectral ratio between horizontal and vertical components of microtremor. Bull Seism Soc Am 88(1):228–241

Lachet C, Bard P-Y (1994) Numerical and theoretical investigations on the possibilities and limitations of Nakamura's technique. J Phys Earth 42:377–397

Lachet C, Hatzfeld D, Bard P-Y, Theodulidis N, Papaioannou C, Savvaidis A (1996) Site effects and microzonation in the city of Thessaloniki (Greece): comparison of different approaches. Bull Seism Soc Am 86:1692–1703

Langston CA (1979) Structure under Mount Rainier, Washington, inferred from teleseismic body waves. J Geophys Res 84:4749–4762

Lermo J, Chávez-García FJ (1993) Site effects evaluation using spectral ratios with only one station. Bull Seism Soc Am 83:1574–1594

Lermo J, Chávez-García FJ (1994) Are microtremors useful in site response evaluation? Bull Seism Soc Am 84:1350–1364

Macias M, Atkinson GM, Motazedian D (2008) Ground-motion attenuation, source, and site effects for the 26 September 2003 M8.1 Tokachi-Oki Earthquake sequence. Bull Seism Soc Am 98(4):1947–1963

Midorikawa S, Miura H, Atsumi T (2012) Strong motion records from the 20122 off pacific coast of Tohoku earthquake. In: Proceedings of the international symposium on engineering lessons learned from the (2011) Great East Japan earthquake, March 1–4, 2012. Tokyo, Japan

Nakamura Y (1989) A method for dynamic characteristics estimation of subsurface using microtremor on the ground surface. Q Rep RTRI 30:25–33

Nogoshi M, Igarashi T (1971) On the amplitude characteristics of microtremor. Part 2. Zisin (J. Seism. Soc. Japan) 24, 26–40 (in Japanese with English abstract)

Ohmachi T, Nakamura Y, Toshinawa T (1991) Ground motion characteristics in the San Francisco Bay area detected by microtremor measurements. In: Prakash S (ed) Proceedings of the second international con-

ference on recent advances in geotechnical earthquake engineering and soil dynamics, St. Louis, Missouri, University of Missouri-Rolla, pp 1643–1648, March 11–15, 1991

Safak E (1991) Problems with using spectral ratios to estimate site amplification. In Proceedings of the fourth international conference on seismic zonation, vol II. EERI, Oakland, pp 277–284

Safak E (1997) Models and methods to characterize site amplification from a pair of records. Earthquake Spectra, EERI 13(1):97–129

Sato K, Kokusho T, Matsumoto M, Yamada E (1996) Nonlinear seismic response and soil property during strong motion. In: Special Issue of Soils and Foundations in Geotechnical Aspects of the January 17. Hyogoken-Nambu Earthquakes, pp 41–52

Satoh T, Kawase H, Sato T (1995) Evaluation of local site effects and their removal from borehole records observed in the Sendai region, Japan. Bull Seism Soc Am 85:1770–1789

Satoh T, Fushimi M, Tatsumi Y (2001a) Inversion of strain-dependent nonlinear characteristics of soils using weak and strong motions observed by boreholes sites in Japan. Bull Seism Soc Am 91:365–380

Satoh T, Kawase H, Matsushima S (2001b) Estimation of S-wave velocity structures in and around the Sendai basin, Japan, using array records of microtremors. Bull Seism Soc Am 91:206–218

Sawazaki K, Sato H, Nakahara H, Nishimura T (2006) Temporal change in site response caused by earthquake strong motion as revealed from coda spectral ratio measurement. Geophys Res Lett 33:L21303

Sawazaki K, Sato H, Nakahara H, Nishimura T (2009) Time-lapse changes of seismic velocity in the shallow ground caused by strong ground motion shock of the 2000 Western-Tottori earthquake, Japan, as revealed from coda deconvolution analysis. Bull Seism Soc Am 99:352–366

Schnabel PB, Lysmer J, Seed HB (1972) SHAKE: a computer program for earthquake response analysis of horizontally layered sites. Technical Report Rept. EERC 72–12, Earthquake Engineering Research Center, University of California, Berkeley

Seed HB, Idriss IM (1970) Analyses of ground motions at Union Bay, Seattle during earthquakes and distant nuclear blasts. Bull Seism Soc Am 60:125–136

Shearer PM, Orcutt JA (1987) Surface and near-surface effects on seismic waves—theory and borehole seismometer results. Bull Seism Soc Am 77:1168–1196

Silva WJ (1986) Soil response to earthquake ground motion, report prepared for Electric Power Research Institute, EPRI Research Project RP 2556–07

Steidl JH (1993) Variation of site response at the UCSB dense array of portable accelerometers. Earthquake Spectra 9:289–302

Steidl JH, Tumarkin AG, Archuleta RJ (1996) What is a reference site? Bull Seism Soc Am 86:1733–1748

Su F, Anderson JG, Brune JN, Zeng Y (1996) A comparison of direct S-wave and coda wave site amplification determined from aftershocks of Little Skull Mountain earthquake. Bull Seism Soc Am 86:1006–1018

Theodulidis N, Bard P-Y (1995) Horizontal to vertical spectral ratio and geological conditions: an analysis of strong motion data from Greece and Taiwan (SMART-I). Soil Dyn Earthq Eng 14:177–197

Theodulidis N, Bard P-Y, Archuleta RJ, Bouchon M (1996) Horizontal-to-vertical spectra ratio and geological conditions: the case of Garner valley downhole array in southern California. Bull Seism Soc Am 86:306–319

Thompson EM, Baise LG, Kayen RE, Guzina BB (2009) Impediments to predicting site response: seismic property estimation and modeling simplifications. Bull Seism Soc Am 99:2927–2949

Thomson WT (1950) Transmission of elastic waves through a stratified solid. J Appl Phys 21:89–93

Tokimatsu K, Tamura S, Suzuki H, Katsumata K (2011) Quick report on geotechnical problems in the 2011 Tohoku Pacific Ocean Earthquake. Res Rep Earthq Eng CUEE Tokyo Inst Technol 118:21–47

Wen K, Beresnev I, Yeh YT (1994) Nonlinear soil amplification inferred from downhole strong seismic motion data. Geophys Res Lett 21:2625–2628

Wu C, Peng Z, Assimaki D (2009) Temporal changes in site response associated with strong ground motion of 2004 M6.6 mid-Niigata earthquake sequences in Japan. Bull Seism Soc Am 99:3487–3495

Wu C, Peng Z, Ben-Zion Y (2010) Refined thresholds for nonlinear ground motion and temporal changes of site response associated with medium size earthquakes. Geophys J Int 183:1567–1576

Wu C, Peng Z, Wang W, Chen Q-F (2011) Dynamic triggering of shallow earthquakes near Beijing, China. Geophys J Int 185:1321–1334

Zeghal M, Elgamal AW (1994) Analysis of site liquefaction using earthquake records. J Geotech Eng 120(6):996–1017

Zerva A, Petropulu AP, Abeyratne U (1995) Blind deconvolution of seismic signals in site response analysis. In: Proceedings of the fifth international conference on seismic zonation, Nice, France

Zhao JX (1996) Estimating modal parameters for a simple soft-soil site having a linear distribution of shear wave velocity with depth. Earthq Eng Struct Dyn 25:163–178

Zhao JX (1997) Modal analysis of soft-soil sites including radiation damping. Earthq Eng Struct Dyn 26: 93–113

Zhao JX, Irikura K, Zhang J, Fukushima Y, Somerville PG, Asano A, Ohno Y, Oouchi T, Takahashi T, Ogawa H (2006a) An empirical site-classification method for strong-motion stations in Japan using H/V response spectral ratio. Bull Seism Soc Am 96:914–925

Zhao JX, Zhang J, Asano A, Ohno Y, Oouchi T, Takahashi T, Ogawa H, Irikura K, Thio HK, Somerville PG, Fukushima Y, Fukushima Y (2006b) Attenuation relations of strong ground motion in Japan using site classification based on predominant period. Bull Seism Soc Am 96:898–913

Zhao JX, Xu H (2012a) Magnitude-scaling rate in ground-motion prediction equations for response spectra from large subduction interface earthquakes in Japan. Bull Seism Soc Am 102:222–235

Zhao JX, Xu H (2012b) A comparison of v_{S30} and site period as site effect parameters in response spectral ground-motion prediction equations. Bull Seism Soc Am (in press)